FLUID MECHANICS PROGRAM
ENGINEERING RESEARCH CENTER
COLLEGE OF ENGINEERING

COLORADO STATE UNIVERSITY
FORT COLLINS, COLORADO

Technical Report

VELOCITY DISTRIBUTIONS IN THE SEPARATED FLOW BEHIND A WEDGE SHAPED MODEL HILL

by

Shih-Cheng Chang

Prepared under

U. S. Army Research Grant DA-AMC-28-043-G20
U. S. Army Materiel Command
Washington 25, D. C.

Fluid Mechanics Program
College of Engineering
Colorado State University
Fort Collins, Colorado

March 1966

CER65SCC66

ABSTRACT OF THESIS

VELOCITY DISTRIBUTIONS IN THE SEPARATED FLOW BEHIND A WEDGE SHAPED MODEL HILL

A portion of the velocity distributions in an incompressible turbulent separated flow behind a two-dimensional model hill is investigated experimentally. A 2" x 2" wedge is used as a model hill. The mixing region investigated lies between the crest of the hill where the flow separated, and the reattachment point where the separated flow reattaches itself to the floor.

Gortler's half-jet mixing theory is used to analyze the separated flow which is curved by the action of the pressure gradient across the separated flow. The width of the mixing region was found to spread linearly with the distance as expressed by the half-jet theory. If a suitable similarity parameter is chosen, the theoretical velocity distribution of half-jet agrees satisfactorily with the experiments, except in the region near the floor and directly behind the hill. However, it was found that the similarity parameter is not a constant, but is proportional to the one-half power of the distance

downstream from the hill. Corrections were applied to account for the effects of the initial boundary layer thickness and for the curvature. The corrections are based on Sawyer's first order theory and Kirk's approximation, but the results indicate that these effects should be investigated further.

Shih-Cheng Chang
Civil Engineering Department
Colorado State University
Fort Collins, Colorado
March, 1966

ACKNOWLEDGEMENTS

The writer wishes to express his indebtedness and sincere gratitude to his major professor, Dr. E. J. Plate, who has given invaluable advice and continuous encouragements to the writer in every phase of the work. To the other members of the graduate committee, Dr. J. E. Cermak, Professor V. A. Sandborn, and Dr. H. R. Bailey, the writer gratefully acknowledges their helpful comments and review of the thesis.

The writer also wishes to express his gratitude to Miss Hanae Akari, Mrs. Mary Fox and Mrs. Carolyn Card for their help in drafting and typing, and Mrs. Lilah Roberts for printing the thesis.

Financial assistance, provided by the Integrated Army Meteorological Wind-Tunnel Research Program under Grant DA-AMC-28-043-G20 , is greatly appreciated.

TABLE OF CONTENTS

TABLE OF CONTENTS - continued

LIST OF FIGURES

LIST OF FIGURES - continued

LIST OF SYMBOLS

Symbol	Definition or Description	Dimension*
x, y	Intrinisc Cartesian coordinates with jet axis as x-axis	L
X, Y	Reference Cartesian coordinates with wind tunnel floor as X-axis	L
r	Cylindrical polar coordinate in radial direction	L
θ	Cylindrical polar coordinate in angular direction	
y_1	Coordinate of y at the upper edge of mixing region where $\frac{\bar{u}}{\bar{u}_1} = 1$	L
y_2	Coordinate of y at the lower edge of mixing region where $\frac{\bar{u}}{\bar{u}_2} = 1$	L
ℓ	Prandtl's mixing length	L
k	Proportionality constant in the evaluation of turbulent shear stress	
Λ	Momentum transfer length	L
b	Width of the mixing region	L

* F = force, L = length, T = time

V = voltage, C = current, R = resistance

LIST OF SYMBOLS - continued

Symbol	Definition or Description	Dimension
x_o	Displacement of the virtual origin from coordinate origin	L
L	Reference length	L
$\bar{u}$	Time-mean velocity in x-direction	$L\,T^{-1}$
$\bar{v}$	Time-mean velocity in y-direction	$L\,T^{-1}$
u'	Fluctuating velocity component of turbulence in x-direction	$L\,T^{-1}$
v'	Fluctuating velocity component of turbulence in y-direction	$L\,T^{-1}$
u	Instantaneous velocity in x-direction, = $\bar{u} + u'$	$L\,T^{-1}$
U_∞	Free stream velocity, i.e., wind speed in wind tunnel	$L\,T^{-1}$
$\bar{u}_1$, $\bar{v}_1$	Mean velocity component in x and y direction respectively in the upper stream outside the mixing region	$L\,T^{-1}$
$\bar{u}_2$, $\bar{v}_2$	Mean velocity component in x and y direction respectively in the lower stream outside the mixing region	$L\,T^{-1}$
λ	Non-dimensional velocity parameter, = $\dfrac{\bar{u}_1 - \bar{u}_2}{\bar{u}_1 + \bar{u}_2}$	
a	The ratio of the velocity along the x-axis to the free stream velocity	
ρ	Density	$F\,T^2\,L^{-4}$

LIST OF SYMBOLS - continued

Symbol	Definition or Description	Dimension
γ	Specific weight	$F\,L^{-3}$
$\bar{p}$	Time-mean value of static pressure	$F\,L^{-2}$
$\bar{p}_o$	Arbitrary datum pressure	$F\,L^{-2}$
H	Total pressure	$F\,L^{-2}$
h	Reading of pressure transducer corresponding to dynamic pressure	$F\,L^{-2}$
ψ	Stream function	$L^2\,T^{-1}$
τ	Turbulent shear stress	$F\,L^{-2}$
ϵ	Apparent kinematic viscosity in turbulent flow	$L^2\,T^{-1}$
ϵ^*	Apparent kinematic viscosity for the zero curvature $= \frac{\epsilon}{1 - mQ}$	$L^2\,T^{-1}$
η	Transformed variable $= \frac{y}{x}$	
ξ	Similarity variable in half-jet theory, Eq. (3-15) $= \sigma \frac{y}{x}$	
σ	Similarity parameter in ξ	
σ_o	Similarity parameter corresponding to the virtual origin case $= (1 + \frac{x_o}{x})\,\sigma$	

LIST OF SYMBOLS - continued

Symbol	Definition or Description	Dimension
σ^*	Similarity parameter corresponding to the condition of zero curvature, Eq. (3-22)	
R	Radius of curvature	L
Q	A parameter in Eq. (3-19) $= \frac{\bar{u}}{R} \frac{1}{\frac{\partial \bar{u}}{\partial y}}$	
m	Constant in Sawyer's first order theory of turbulent shear stress	
C	Proportionality constant in Eq. (3-8)	
η^* , $\bar{\eta}^*$	Transformed variables in Eq. (2-3)	
η_1 , η_1^*	Value of η and η^* respectively when $y = y_1$	
δ	Half thickness of boundary layer	L
δ_o	Initial boundary layer thickness	L
α , β	Angle at which hot wire inclines to the main stream direction	
R_a	Electric resistance of hot wire at air temperature	R
R_w	Electric resistance of hot wire in operation	R
e'	Voltage across hot wire	V
I	Electric current passing the hot wire	C

LIST OF SYMBOLS - continued

Symbol	Definition or Description	Dimension
I'	Fluctuation of current	C
S	Sensitivity of hot-wire anemometer	$C\ T\ L^{-1}$
A	Calibration constant $= \frac{1}{S}$	$L\ T^{-1}\ C^{-1}$

Any other symbols which do not appear here will be described whenever they first appear.

Chapter I

INTRODUCTION

When air flows along a flat plate, it develops a boundary layer with a thickness that increases with distance. If the air flow encounters an abrupt obstacle, such as a sharp crested hill, the flow field is distorted. The flow separates at the crest of hill and standing eddies appear in front and behind the hill. The separation streamline reattaches to the floor at the reattachment point downstream from the hill. As shown in Fig. 1 , the flow field between the crest of the hill and the reattachment point can be divided roughly into three regions overlaying each other: the separation bubble, the separation region in the neighborhood of the separation streamline, and the free stream region. Within the separation bubble, the velocity is very small and may be considered as being almost zero. In the separation region the velocity varies rapidly from zero to the free stream velocity.

It is the objective of this thesis to investigate this separation region and to determine if it is possible to use an analysis based on the half-jet model of free turbulent shear flow for the velocity distribution in the separation region. The air flow is two dimensional, turbulent and incompressible. The hill is simulated by a constant

cross section wedge 2 x 2 in. placed perpendicular to the flow direction on a wind tunnel floor.

The separated flow can be looked upon as a free turbulent shear flow similar to wakes, jets or half-jets, because both the separated flow and the free turbulent shear flow are similarly characterized by two regions with different velocities and a mixing layer within which the velocity difference is smoothed out. An examination of the characteristic of each type of free turbulent shear flow indicates that the half-jet is the most logical model. The objection to the jet model can be seen from the decrease of the maximum jet velocity with distance, while the maximum velocity in the separated flow is nearly constant. The wake model is not desirable either because the velocity difference between the wake and the free stream diminishes with distance which is not true for the separated flow. Besides, the large downstream distance required by available wake analysis can not be obtained in separated flow. However, the above objections vanish when the half-jet analysis is used. Consequently, the turbulent half-jet mixing flow is employed in this thesis as the model of the separated flow behind a two-dimensional hill and Gortler's half-jet theory is applied to the analysis.

The turbulent half-jet mixing flow has been studied by many investigators. A review of work on the turbulent half-jet problem is

given in Chapter II. However, it is only in recent years that the half-jet mixing layer was employed as the model of separated flow by Chapman (2) and Korst (7) . Since then a considerable amount of work concerning the separated flow in supersonic flow have been based on this model. Such investigations have dealt principally with the base pressure behind blunt bodies and the pressure rise at the reattachment point in supersonic flow. Little has been done to study the half-jet model itself in the analysis of separated flow.

With this in view, this study investigates the nature of the separated flow compared to the half-jet and the half-jet model is verified as usuable for analysis of the separated flow region. In addition, the flow separating at the crest of a model hill exhibits certain features different from conditions found in classical half-jet. The presence of the lower boundary gives rise to a boundary layer into which the obstacle is immersed. The separation phenomenon results in a pressure gradient both in the axial direction and perpendicular to the half-jet flow. An attempt will be made to account for these effects by pointing out possible corrections. A reasonable consistent model is developed whose numerical coefficients are obtained from the experimental results.

Chapter II

REVIEW OF LITERATURE

The purpose of this chapter is to present available information concerning the half-jet mixing of turbulent, incompressible flow and the contributions of various investigators to half-jet analysis. To grasp the full half-jet mixing concept, which is one of the free turbulent shear flow, it is felt that free turbulent shear flow should be discussed first.

A. Free Turbulent Shear Flow

Free turbulent shear flows occur when there is no direct influence of a solid boundary. The effect of viscosity is very small and the flow spreads laterally into the ambient fluid. It has been found that free turbulent shear flow has a nature similar to a boundary layer. This means that:

1. The mean flow velocity transverse to the main flow is very small when compared with the main flow velocity.
2. Changes of quantities in the direction of the main flow are correspondingly slow with respect to those in the transverse direction.

3. The mean pressure variation across the flow region in the transverse direction is small.

Consequently, the equation of motion for a boundary layer, can be used to analyze a two-dimensional free turbulent flow of an incompressible fluid. For the steady case, the equation is

$$\bar{u}\frac{\partial \bar{u}}{\partial x} + \bar{v}\frac{\partial \bar{u}}{\partial y} = -\frac{1}{\rho}\frac{\partial \bar{p}}{\partial x} + \frac{1}{\rho}\frac{\partial \tau}{\partial y} \qquad (2\text{-}1)$$

B. W. Tollmien's Analysis and Kuethe's Extention

Many investigations have been carried out in an attempt to gain a knowledge concerning the behavior of turbulent mixing in an incompressible fluid. In 1926, W. Tollmien (26) was the first to succeed in the analyzing of a turbulent mixing flow. He worked out three different types of mixing: half-jet, plane jet and axially symmetric jet. The half-jet is a parallel stream mixing with the adjacent fluid at rest. A plane jet is formed by a two-dimensional jet issuing from a narrow opening into a fluid at rest. In his analysis of the turbulent half-jet with zero pressure gradient, W. Tollmien employed the mixing length theory and showed that the width of the turbulent jet increased linearly with x. He then used the equation:

$$\bar{u}\frac{\partial \bar{u}}{\partial x} + \bar{v}\frac{\partial \bar{u}}{\partial y} = 2l^2\frac{\partial \bar{u}}{\partial y}\frac{\partial^2 \bar{u}}{\partial y^2} \qquad (2\text{-}2)$$

in which the mixing length ℓ is assumed to be proportional to the distance $\ell = cx$, c is a constant to be determined from experiments. By introducing a stream function $\psi = \int \bar{u}\, dy$ and new variables successively

$$\bar{\eta}^* = \eta^* - \eta_1^*, \quad \eta^* = \frac{\eta}{(2c^2)^{\frac{1}{3}}}, \quad \eta = \frac{y}{x}$$

he obtained the solution $\bar{u} = \bar{u}_1 F'(\eta)$ where the prime denotes differentiation with respect to η and

$$F = d_1 e^{-\bar{\eta}^*} + d_2 e^{\bar{\eta}^*/2} \cos\left(\sqrt{\frac{3}{2}}\,\bar{\eta}^*\right) + d_3 e^{\bar{\eta}^*/2} \sin\left(\sqrt{\frac{3}{2}}\,\bar{\eta}^*\right) \tag{2-3}$$

With application of boundary conditions

at the inner edge $\eta = \eta_1$	$\bar{u} = \bar{u}_1$	$F' = 1$
	$\frac{\partial \bar{u}}{\partial y} = 0$	$F'' = 0$
	$\bar{v} = 0$	$F = \eta_1$
at the outer edge $\eta = \eta_2$	$\bar{u} = 0$	$F' = 0$
	$\frac{\partial \bar{u}}{\partial y} = 0$	$F'' = 0$

coefficients in the solution were

$$d_1 = -0.0062 \qquad d_2 = 0.987 \qquad d_3 = 0.577 \tag{2-4}$$

$$\eta_1^* = 0.981 \qquad \eta_2^* = -2.04$$

c was found from experiment to be 0.0174 .

Tollmien's solution has been verified by Liepmann and Laufer (9) , who measured the mean velocity distribution in a half-jet. Good agreement was found between theory and measurements. For plane jet analysis W. Tollmien expressed his solution as:

$$\bar{u} = \frac{1}{\sqrt{x}} F'(\eta)$$

$$F(\eta^*) = e^t \qquad Z(\eta) = t'(\eta) \tag{2-5}$$

$$\eta = \frac{\pi}{\sqrt{3}} - \frac{2}{3}\left\{\log(\sqrt{Z}+1) - \log\sqrt{(Z-\sqrt{Z}+1)} + \sqrt{3}\tan^{-1}\left(\frac{2\sqrt{Z}-1}{\sqrt{3}}\right)\right\}$$

This theoretical solution gave a zero radius of curvature at the axis of the jet, $\eta^* = 0$, which is a defect in Tollmien's solution. Later analysis such as Gortler's results improved this point. Forthmann (4) made an experimental measurement of a plane jet which showed good agreement between measured velocity profiles and Tollmien's solution, except near the axis of the jet. There are several noteworthy assumptions in Tollmien's analysis:

1. The ambient fluid is at rest.

2. Prandtle's mixing length theory is employed.

$$\tau = -\rho \overline{u'v'} = \rho \ell^2 \left|\frac{\partial \bar{u}}{\partial y}\right| \frac{\partial \bar{u}}{\partial y}$$

the mixing length ℓ is assumed constant across the width of mixing region and proportional to the distance $\ell = cx$.

3. The pressure gradient in the main stream direction is assumed to be zero $\frac{\partial \bar{p}}{\partial x} = 0$.
4. A uniform initial velocity distribution before mixing is assumed, so that the initial boundary layer thickness is not considered.
5. The width of the mixing region increases linearly with distance.
6. Similarity of velocity is assumed.

If any one of the above assumptions is changed, a new solution will be required. Hence, the introduction of new boundary conditions; such as the surrounding fluid being in motion, or the application of a new turbulent shearing stress hypothesis, or consideration of an initial boundary layer; form the core of subsequent development in the turbulent mixing flow.

In 1935, Kuethe (8) extended Tollmien's solution to a general case of the mixing of two parallel streams of different velocities. The differential equation and its solutions are the same as Tollmien's half-jet analysis. Two different boundary conditions were introduced (1) $\bar{u} = \bar{u}_2$ at $\eta = \eta_2$, corresponding to an ambient fluid with a

velocity $\bar{u}_2$ and (2) (suggested by Von Karman) $\bar{u}_1\bar{v}_1 = -\bar{u}_2\bar{v}_2$. This corresponds to the assumption that no external forces perpendicular to the main flow are acting on the total fluid system. Kuethe found that the effect of the boundary condition change from $\bar{u}_2 = 0$ to $\bar{u}_2 \neq 0$ is very small. Neither the mixing region width nor the velocity profiles were affected. The effect can be seen only from a slight displacement in the position of the edge. In 1944, Squire and Trouncer (25) worked out the case of the axially symmetrical jet issuing into a uniform stream.

C. Reichardt's Inductive Theory and Gortler's Analysis

One common feature seen in all turbulent studies is that a suitable assumption must be made for the unknown relation between the turbulent shear stress and the mean motion. The results based on these assumptions are then checked by a final comparison with experimental results. It turned out that the results obtained from each turbulence theory did not differ to any great extent. This indicates that the mean velocity distribution is insensitive to the form assumed for the turbulent shear stress. Reichardt (18) in 1941, therefore, suggested an inductive theory. Instead of beginning with a hypothesis on the mixing length or shear stress, he critically examined the voluminous experimental data on free turbulent shear flows, and discovered that the velocity profiles under consideration

could be approximated very successfully by the error function or Gauss's function. He also found empirically that if there was a relation such as $\overline{uv} = -\Lambda(x) \frac{\partial \bar{u}^2}{\partial y}$, then an equation describing the velocity distribution in the free turbulent flow can be obtained

$$\frac{\partial \bar{u}^2}{\partial x} = \Lambda(x) \frac{\partial^2 \bar{u}^2}{\partial y^2} \qquad (2\text{-}6)$$

Here $\Lambda(x)$ has the dimension of a length and must be determined experimentally. This equation for free turbulence is identical to the well known one-dimensional heat conduction equation, which yields the error or Gauss function as a solution. Thus, an analogy was found between turbulent transfer and heat conduction. The empirical relation $\overline{uv} = -\Lambda \frac{\partial \bar{u}^2}{\partial y}$ is then an expression of the law of momentum transfer which states that the flux of the x-component of momentum, which is transferred in a transverse direction, is proportional to the transverse gradient of momentum. According to Fourier's law of heat conduction, the heat flux is proportional to the temperature gradient. $\Lambda(x)$ is then analogous to the heat conductivity and might be termed as a momentum transfer length. As a consequence, the differential equation of heat conduction can be applied to turbulent transfer of momentum. This hypothesis essentially means that the exchange coefficient ϵ is constant across each section of the turbulent mixing region (14). The turbulent exchange coefficient ϵ is

defined as $\epsilon = -\ell\bar{v}'$. Prandtl suggested that when using this hypothesis $\epsilon = kb\,(\bar{U}_{max} - \bar{U}_{min})$ where b is the width of the mixing zone, and k is a dimensionless proportional factor. The new hypothesis of constant exchange coefficient was employed by H. Gortler (23) in 1942 to re-examine Tollmien's problem. A much simpler mathematical solution to the half-jet case was obtained with a first order approximation, which showed good agreement with the experiments of H. Reichardt. For a uniform stream mixing with a fluid at rest, his analysis provided a velocity distribution expressed by the error function

$$\frac{\bar{u}}{u_1} = \frac{1}{2}(1 + \operatorname{erf} \xi) \qquad (2\text{-}7)$$

where

$\xi = \sigma \frac{y}{x}$ and σ is a constant of proportionality.

Because of its simplicity, this equation has been used widely in the analysis of separation flow (11) and in the analysis of base pressure problems (2) . The zero radius of curvature of velocity profile as expressed in Tollmien's analysis of plane jet is improved when Eq. (2-7) is employed. However, the theoretical mean velocity near the edge of the mixing layer is higher than the experimental value.

D. Dimensional Argument

Most analyses of free turbulent flows are based on some hypothesis for the mechanism of turbulence, such as constant mixing length, or constant exchange coefficient. However, these assumptions are not always in agreement with measurements. In 1947, Liepmann and Laufer (9) made an experimental investigation of free turbulent mixing in a half-jet. They measured turbulent shearing stress and the mean velocity profiles across the width of a mixing region. Then, the mixing length and the exchange coefficients were computed across the width. Liepmann and Laufer found that both the mixing length and the exchange coefficient were not constant, but varied across the mixing region. Consequently, they concluded that Tollmien and Gortler's theory were based on invalid assumptions.

For many years, there has been a growing realization that dimensional analysis can furnish practically all the results of any mixing theories. C. B. Millikan (12) and Squire (24) all have expressed this point of view.

In 1945, Squire has shown that all the results about the mean quantities in free turbulent shear flow can be deduced by means of a dimensional analysis, without introducing any hypothesis for the turbulent mechanism. Two assumptions were made in his analysis. First, the distribution of velocity and shearing stress are similar at

all sections. Second, the shearing stress is proportional to the square of the maximum difference in velocity across a section and is independent of viscosity.

Liepmann and Laufer (9), in their investigation of a half-jet, tried to describe the behavior of turbulent mixing by means of the energy and momentum integral for the mean and fluctuating motion. They reached the same conclusion as Squire, and once more demonstrated that a complete understanding of the physical aspects of turbulent motion is not necessary for the analysis of the free turbulent shear flow. Dimensional reasoning allows investigators to obtain the overall characteristic of the turbulent mixing process.

E. Torda's Analysis and Kirk's Approximation

Previous investigations always assumed a linear variation of the mixing region width with x and a uniform velocity distribution in the stream before mixing without considering the influence of the upstream boundary layer. Besides, the approaches always used the transformation from the x, y-plane into an η-plane, where η is proportional to $\frac{y}{x}$. The boundaries of the mixing region corresponding to the constant values of η turned out to be straight lines owing to the transformation used. In order to consider the effect of upstream boundary layer, Torda (27) in 1953 used an alternate approach in his analysis of symmetric turbulent mixing of two parallel streams. Both

streams, which were separated by an infinite thin plate before mixing, had the same velocity distribution with the boundary layer existing. Torda used a quartic polynomial, which satisfied all the boundary conditions, as an approximation of the velocity profile in the mixing zone.

$$\frac{\bar{u}}{\bar{u}_1} = a(\eta^2 - 1)^2 - (\eta^2 - 2)\eta^2 \qquad (2\text{-}8)$$

where $\eta = \frac{y}{x}$, $a = \frac{\bar{u}_{y=0}}{\bar{u}_1}$ is a non-dimensional velocity along the x-axis. Boundary conditions are

$$y = \pm\delta \qquad \bar{u} = \bar{u}_1 \qquad \frac{\partial \bar{u}}{\partial y} = 0$$

$$y = 0 \qquad \frac{\partial \bar{u}}{\partial y} = 0$$

Then the integral equation for the momentum and energy equation was applied . The constant exchange coefficient was also used for the turbulent shear stress. With the application of boundary conditions, the following equations were obtained.

$$\frac{d}{dx}\int_0^{\delta} \bar{u}^2\, dy - \bar{u}_1 \frac{d}{dx}\int_0^{\delta} \bar{u}\, dy = 0 \qquad (2\text{-}9)$$

$$\frac{1}{2}\frac{d}{dx}\int_0^{\delta} \bar{u}^3\, dy - \frac{\bar{u}_1^2}{2}\frac{d}{dx}\int_0^{\delta} \bar{u}\, dy +$$

$$+ kb(x)\,\bar{u}_1\,(1-a)\int_0^{\delta}\left(\frac{\partial \bar{u}}{\partial y}\right)^2 dy = 0 \qquad (2\text{-}10)$$

Substituting Eq. (2-8) into Eq. (2-9) and Eq. (2-10) yields the thickness of the mixing region as a function of x.

$$\delta(x) = \frac{c_1}{16a^2 - 11a - 5} \qquad (2\text{-}11)$$

where a is the function of x, which can be evaluated graphically from the following integration:

$$\int_0^{a} \frac{640a^4 - 880a^3 - 119a^2 + 478a - 39}{572(a-1)^3\,(16a^2 - 11a - 5)^2}\, da = \frac{k}{c_1}(x + c_2) \qquad (2\text{-}12)$$

in which c_1 and c_2 are constants to be determined from experiments. Thus, from Eq. (2-11), the boundaries of the mixing zone are no longer straight lines but are curved and the curvature starts in the region immediately behind the plate. However, far downstream the velocity profiles in the mixing zone tend to become similar and the boundaries of the turbulent mixing zone tend to be straight lines as is expected.

In 1959, Kirk (6) suggested an approximate method to include the effect of the initial boundary layer thickness in his study of base pressure in supersonic flow. He displaced the origin of the mixing region upstream to a virtual origin and assumed that the turbulent mixing started to develop from the virtual origin instead of the true origin. He was then able to obtain a similar profile in the mixing region.

F. Sabin's Analysis

The analyses of turbulent mixing discussed above were all based on the assumption that no pressure gradient exists in the main stream. In practice this is not exactly true. In 1963, C. M. Sabin (20) took a pressure gradient in the x-direction into consideration, while he studied the free turbulent mixing between two parallel streams with different velocities. Sabin did not assume a pressure gradient across the mixing region in the transverse direction. Realizing that different hypotheses of turbulent shearing stress always lead to a different form of solution, Sabin intended to derive a general solution for any turbulent shear stress hypothesis as well as for arbitrary pressure gradient in the main stream direction. For this purpose he used a series of coordinate transformations to absorb the effect of the pressure gradient $\frac{\partial \bar{p}}{\partial x}$ and the apparent kinematic

viscosity ϵ . He began with the equation of motion

$$\bar{u}\frac{\partial \bar{u}}{\partial x} + \bar{v}\frac{\partial \bar{u}}{\partial y} = -\frac{1}{\rho}\frac{\partial \bar{p}}{\partial x} + \epsilon\frac{\partial^2 \bar{u}}{\partial y^2} \quad ,$$

then introduced the following transformations:

$$P = \bar{p}(x) - \bar{p}_o + \frac{1}{2}\rho\,\bar{u}^2$$

$$\bar{P} = \frac{P}{\frac{1}{2}(P_1 + P_2)}$$

$$\bar{x} = \frac{x}{L} \qquad \bar{y} = \frac{y}{L} \tag{2-13}$$

$$\bar{\epsilon} = \frac{\epsilon}{UL} \qquad \bar{\psi} = \frac{\psi}{UL} \qquad U = \left[\frac{1}{\rho}(P_1 + P_2)\right]^{\frac{1}{2}}$$

$$\hat{x} = \int_o^{\bar{x}} \bar{\epsilon}(t)\,dt \qquad \hat{\psi} = \bar{\psi}$$

Where ψ is the stream function, U is reference velocity, L is reference length, $\bar{p}_o$ is datum pressure and P is total pressure; subscript 1 refers to the upper free stream and 2 corresponds to the lower free stream. The equation of motion was finally reduced to a simplified form

$$\frac{\partial \bar{P}}{\partial \hat{x}} = \left(\frac{\bar{u}}{U}\right)\frac{\partial^2 \bar{P}}{\partial \hat{\psi}^2} \tag{2-14}$$

In which both the pressure gradient and apparent kinematic viscosity disappeared. A solution which is self-similar was obtained for the first order approximation

$$\frac{\bar{u}^2}{\frac{1}{2}(\bar{u}_1^2 + \bar{u}_2^2)} = 1 + \frac{\bar{u}_1^2 - \bar{u}_2^2}{\bar{u}_1^2 + \bar{u}_2^2} \operatorname{erf} \eta \qquad (2\text{-}15)$$

where

$$\eta = \frac{\hat{\psi}}{2(\phi + \phi_o)^{1/2}}$$

$$\phi = \int_o^{\bar{x}} \frac{1}{2}(\bar{u}_1^2 + \bar{u}_2^2)^{\frac{1}{2}} \frac{\bar{\epsilon}(t)}{U} dt$$

ϕ_o is an integral constant.

This solution is independent of the particular choice of either the pressure gradient or apparent kinematic viscosity. The dimensionless velocity profile in the mixing region is found to be a function of the velocity ratio of two parallel streams only. Velocity profile obtained by this theory was compared with those obtained by the Gortler's theory for the case of a zero pressure gradient. Satisfactory agreement is obtained when the velocity ratio of the slow stream to the fast stream is greater than 0.5 . However, if the

velocity ratio is small, lower than 0.4, the agreement can not be expected, because the simplifications that were introduced in the process of comparison are no longer permissible. An interesting note in Sabin's analysis is that the apparent kinematic viscosity is insensitive to the pressure gradient in main stream direction. Sabin concluded that Prandtl's hypothesis $\epsilon = kb(\bar{u}_{max} - \bar{u}_{min})$ is adequate also for a free jet flow with an arbitrary longitudinal pressure gradient.

G. Sawyer's First Order Theory

In 1960, Sawyer (21) conducted an investigation of a curved two-dimensional turbulent jet discharging parallel to a flat plate at some distance from the plate. He found that the measured velocity profiles of the jet as it curved toward the plate, were nearly symmetrical; although there was a pressure difference across the jet. The total rate of jet spread was almost identical to that of a plane jet. It seemed that the curvature had only a small effect on the velocity distribution in the jet. In order to get a deeper insight into this effect, Sawyer (22) extended the mixing length concept to include the effect of the curvature, and derived a first order theory for turbulent shearing stress.

$$\tau = \rho\epsilon^* \left| \frac{\partial \bar{u}}{\partial y} - m \frac{\bar{u}}{R} \right| \qquad (2\text{-}16)$$

where ϵ^* is the apparent kinematic viscosity for zero curvature and R is the radius of curvature.

The first order mixing length theory indicates that the curvature has a considerable effect on the rates of entrainment, but this need not necessarily be accompanied by a marked deviation in the jet velocity profile from that of a plane jet, since there exists a corresponding flow across the locus of the maximum profile velocity, which balanced the effect of different entrainment rates.

H. Chapman and Korst's Analysis

Another theory similar to Torda's, which deals with the effects of the initial boundary layer on the mixing within a half-jet, was derived by A. J. Chapman and H. H. Korst in 1954 (1) . Their basic approach followed the Pai analysis of jet mixing of a compressible fluid. The one exception to this approach was that they included the initial boundary layer. Pai (15) in 1949, proposed a small perturbation method to linearize the equation of motion within the mixing region. Thus, the equation of motion was simplified to a form identical to that of the heat conduction equation.

$$\frac{\partial \bar{u}}{\partial \xi_o} = \frac{\epsilon_o}{\bar{u}_1} \frac{\partial^2 \bar{u}}{\partial y^2} \tag{2-17}$$

where $\xi_o = \frac{x^{n+1}}{(n+1)\,L^n}$ n lies between 0 and 1 and the exact value of n depends on the condition of mixing.

ϵ_o is the empirical constant determined from experiments

L is character length.

Pai also proposed a representation of apparent kinematic viscosity in the form $\epsilon = \epsilon_o \left(\frac{x}{L}\right)^n$. This simplified equation of motion was applied by Chapman and Korst to the problem of the half-jet, with the following boundary conditions.

$$\begin{aligned}
x = 0 \qquad & \frac{\bar{u}}{\bar{u}_1} = 0 && \text{for } -\infty < y < 0 \\
& = f\left(\frac{y}{\delta_o}\right) && \text{for } 0 < y < \delta_o \\
& = 1 && \text{for } \delta_o < y < \infty \qquad (2\text{-}18) \\
x = x \qquad & \frac{\bar{u}}{\bar{u}_1} \longrightarrow 0 && \text{for } y \longrightarrow -\infty \\
& \frac{\bar{u}}{\bar{u}_1} \longrightarrow 1 && \text{for } y \longrightarrow +\infty
\end{aligned}$$

where δ_o is the initial boundary layer thickness. They obtained the following solution:

$$\frac{\bar{u}}{\bar{u}_1} = \frac{1}{2}\left[1 + \operatorname{erf}(\eta - \eta_o) + \frac{1}{\sqrt{\pi}} \int_{\eta-\eta_o}^{\eta} f\left(\frac{\eta-t}{\eta_o}\right) e^{-t^2}\, dt\right] \qquad (2\text{-}19)$$

in which the dimensionless variables η and η_o are written as

$$\eta = y \left(\frac{\bar{u}_1}{4\epsilon_o \xi_o}\right)^{\frac{1}{2}}$$

$$\eta_o = \delta_o \left(\frac{\bar{u}_1}{4\epsilon_o \xi_o}\right)^{\frac{1}{2}}$$

If the thickness of the initial boundary layer is very thin when compared with the length of the wake, then $\eta_o = 0$. The solution reduced to

$$\frac{\bar{u}}{\bar{u}_1} = \frac{1}{2}(1 + \operatorname{erf} \eta) \qquad (2\text{-}20)$$

This solution is identical to that obtained by Gortler using the alternative approach, for a half-jet with no initial boundary layer. Equation (2-20) was adopted in various studies related to the free turbulent shear flow. Korst (7), in his investigation of base pressure

in transonic and supersonic flow, applied this equation to describe the motion of a half-jet mixing and succeeded in establishing a criterion for the reattachment pressure rise in terms of the total pressure developed along the separation streamline. Mueller (13) and McDonald (11), also used this distribution of velocity in their investigations of turbulent separation flow, and achieved satisfactory results. In view of the successful applications made by previous investigators, the same equation is employed throughout this investigation of velocity profiles along the separation region.

Chapter III

THEORETICAL BACKGROUND

This thesis employes a turbulent half-jet mixing flow as a model of the flow along the separation region behind a two-dimensional hill. It is the purpose of this chapter to present a theoretical review of half-jet analysis following the work of Gortler.

Suppose two parallel streams of different velocities, $\bar{u}_1$ and $\bar{u}_2$, are separated by a thin plate along the negative x-axis and come into contact at $x = 0$ (see Fig. 2). Downstream from this point a turbulent mixing region will occur. The velocity of upper stream is $\bar{u}_1$ which is larger than the lower stream velocity $\bar{u}_2$.

The equation of motion for free turbulent shear flow in steady state is

$$\bar{u}\frac{\partial \bar{u}}{\partial x} + \bar{v}\frac{\partial \bar{u}}{\partial y} = -\frac{1}{\rho}\frac{\partial \bar{p}}{\partial x} + \frac{1}{\rho}\frac{\partial \tau}{\partial y} \qquad (3\text{-}1)$$

The pressure gradient in x-direction is assumed negligible and Prandtl's hypothesis of constant exchange coefficient is used for turbulent shear stress $\tau = \rho\epsilon\frac{\partial \bar{u}}{\partial y}$.

$$\epsilon = kb(\bar{U}_{max} - \bar{U}_{min}) = kb(\bar{u}_1 - \bar{u}_2) \qquad (3\text{-}2)$$

where b is the width of the mixing region and k is the constant. Eq. (3-1) reduces to

$$\bar{u}\frac{\partial \bar{u}}{\partial x} + \bar{v}\frac{\partial \bar{u}}{\partial y} = kb\,(\bar{u}_1 - \bar{u}_2)\frac{\partial^2 \bar{u}}{\partial y^2} \tag{3-3}$$

The equation of continuity is

$$\frac{\partial \bar{u}}{\partial x} + \frac{\partial \bar{v}}{\partial y} = 0 \tag{3-4}$$

The required boundary conditions are

$$\begin{aligned} y &= +\infty \qquad \bar{u} = \bar{u}_1 \\ y &= -\infty \qquad \bar{u} = \bar{u}_2 \end{aligned} \tag{3-5}$$

Introduction of the stream function ψ will eliminate the continuity equation, and transform Eq. (3-3) into

$$\frac{\partial \psi}{\partial y}\frac{\partial^2 \psi}{\partial x \partial y} - \frac{\partial \psi}{\partial x}\frac{\partial^2 \psi}{\partial y^2} = kb\,(\bar{u}_1 - \bar{u}_2)\frac{\partial^3 \psi}{\partial y^3} \tag{3-6}$$

putting $\xi = \sigma \dfrac{y}{x}$

and $\psi = \dfrac{1}{2}(\bar{u}_1 + \bar{u}_2) \times f(\xi)$

where σ is an arbitrary constant

then $\bar{u} = \dfrac{\sigma}{2}(\bar{u}_1 + \bar{u}_2)\, f'(\xi)$

Equation (3-6) leads to the following differential equation for $f(\xi)$

$$f(\xi)\, f''(\xi) + 2\,\frac{k\sigma b}{x}\,\frac{\bar{u}_1 - \bar{u}_2}{\bar{u}_1 + \bar{u}_2}\, f'''(\xi) = 0 \qquad (3\text{-}7)$$

let $$\lambda = \frac{\bar{u}_1 - \bar{u}_2}{\bar{u}_1 + \bar{u}_2}$$

and assume that the mixing region width is proportional to distance

$$b = cx \qquad (3\text{-}8)$$

where c is a proportional constant.

Equation (3-7) finally takes the form of

$$f'''(\xi) + 2\sigma f(\xi)\, f''(\xi) = 0 \qquad (3\text{-}9)$$

with $$\sigma = \frac{1}{2\sqrt{kc\lambda}}$$

The new boundary conditions correspondingly are

$$\begin{aligned} \xi &\longrightarrow +\infty \qquad & \sigma f'(\xi) &= 1 + \lambda \\ \xi &\longrightarrow -\infty \qquad & \sigma f'(\xi) &= 1 - \lambda \end{aligned} \qquad (3\text{-}10)$$

The differential Eq. (3-9) is identical to the Blasius equation for a flat plate at zero incidence, with different boundary conditions.

THIS
PAGE
IS
MISSING
IN
ORIGINAL
DOCUMENT

is given by the error function

$$f_1'(\xi) = \frac{2}{\sqrt{\pi}} \int_0^{\xi} e^{-\xi^2} d\xi = \text{erf}\, \xi \tag{3-13}$$

in which the boundary conditions have been utilized. Now the velocity distribution across the mixing region for the first order approximation can be written as

$$\bar{u} = \frac{\bar{u}_1 + \bar{u}_2}{2} \left[1 + \frac{\bar{u}_1 - \bar{u}_2}{\bar{u}_1 + \bar{u}_2} \text{erf}\, \xi \right] \tag{3-14}$$

If it is assumed that $\bar{u}_2 = 0$, which corresponds to the case of a uniform free stream mixing with a fluid at rest, then Eq. (3-14) reduces to

$$\frac{\bar{u}}{\bar{u}_1} = \frac{1}{2}(1 + \text{erf}\, \xi) \tag{3-15}$$

where $\xi = \sigma \frac{y}{x}$

The parameter σ is a constant which must be determined experimentally to give the best agreement between theory and measurements. Eq. (3-15) is the basic equation for a half-jet mixing region, and is used to analyze the separated flow in this investigation. When deriving Eq. (3-15) it was assumed that there was no initial boundary

layer thickness, and no pressure gradient across the mixing region in the direction normal to the main stream.

When considering the effect of the initial boundary layer thickness, the approximation method suggested by Kirk (6) can be adopted by displacing the origin of a half-jet from the crest of the model hill to a virtual origin with a distance x_o upstream of the original origin. Thus, the half-jet was assumed to have developed from the virtual origin instead of from the hill crest. Let σ_o be the similarity parameter for the case of the virtual origin, then the velocity profiles in the mixing region are represented as

$$\frac{\bar{u}}{\bar{u}_1} = \frac{1}{2}\left[1 + \operatorname{erf}\left(\sigma_o \frac{y}{x + x_o}\right)\right] \tag{3-16}$$

From Eq. (3-15) and Eq. (3-16), the relation between σ and σ_o is obtained

$$\sigma = \frac{\sigma_o}{1 + \frac{x_o}{x}} \tag{3-17}$$

Equation (3-17) indicates that σ will increase with distance x if σ_o is constant. A normal pressure gradient across the mixing region always causes the flow field to curve. The effect of this curvature on the turbulent shearing stress has been discussed by

Sawyer (21) who introduced a first order theory which accounts for the effect of this curvature. He expressed the turbulent shearing stress as

$$\tau = \rho \epsilon^* \left[\frac{\partial \bar{u}}{\partial y} - m \frac{\bar{u}}{R}\right] \tag{3-18}$$

where R is the radius of the curvature, ϵ^* is the apparent kinematic viscosity for the zero curvature, and m is an empirical constant which Sawyer found as 5 . Equation (3-18) can be re-written as

$$\tau = \rho \epsilon^* \left[1 - m \frac{\bar{u}}{R} \frac{1}{\frac{\partial \bar{u}}{\partial y}}\right] \frac{\partial \bar{u}}{\partial y} = \rho \epsilon \frac{\partial \bar{u}}{\partial y}$$

The effect of a curvature is seen in the apparent kinematic viscosity

$$\epsilon = \epsilon^* (1 - mQ) \tag{3-19}$$

where $Q = \dfrac{\bar{u}}{R} \dfrac{1}{\frac{\partial \bar{u}}{\partial y}}$

From Eq. (3-2) and Eq. (3-8) , it yields

$$\epsilon = k c x (\bar{u}_{max} - \bar{u}_{min})$$

and recall that in Eq. (3-9) , it is assumed

$$\sigma = \frac{1}{2\sqrt{kc\lambda}}$$

$$= \frac{1}{2\sqrt{kc}} \qquad \text{if } \lambda = 1$$

For the case of the zero curvature it will become

$$c^* = (kc)^* \times (\bar{u}_{max} - \bar{u}_{min})$$

$$\sigma^* = \frac{1}{2\sqrt{(kc)^*}}$$

Therefore $$\sigma = \sigma^* \frac{1}{\sqrt{1 - mQ}} \qquad (3\text{-}20)$$

where σ^* is the similarity parameter corresponding to conditions of zero curvature, which is usually taken as 12 for half-jet mixing. The effect of curvature on the similarity parameter is contained in the factor $\frac{1}{\sqrt{1 - mQ}}$.

If the effects due to curvature and initial boundary layer thickness are combined, the similarity parameter σ^* with zero curvature and zero initial boundary layer thickness will be modified by Eq. (3-17) as well as by Eq. (3-20) . From Eq. (3-20), the similarity parameter σ_o with curvature but without initial boundary layer thickness, is obtained.

$$\sigma_o = \sigma^* \frac{1}{\sqrt{1 - m\bar{Q}}} \tag{3-21}$$

which is again modified by Eq. (3-17) to include the effect of the initial boundary layer thickness expressed in terms of the virtual origin displacement x_o .

$$\sigma = \frac{\sigma_o}{1 + \frac{x_o}{x}} = \frac{1}{1 + \frac{x_o}{x}} \cdot \sqrt{1 - m\bar{Q}} \tag{3-22}$$

This equation indicates how the curvature and the initial boundary layer thickness affect the similarity parameter σ . The error law, Equation (3-15) , for describing the velocity distributions in the separated flow region shall be tested and Eq. (3-22) will also be checked whether it suffices to account for the effect of the transverse pressure gradient and of the initial boundary layer.

Chapter IV

EXPERIMENTAL EQUIPMENT AND PROCEDURES

Experiments were performed in a low speed wind tunnel at the Fluid Dynamic and Diffusion Laboratory at Colorado State University. Measured quantities consisted of mean velocity profiles, static pressures, turbulent velocity components and the location of reattachment. The following paragraphs will provide concise information about the equipment and procedures.

A. Wind Tunnel

Experiments were conducted in a closed circulating type wind tunnel as shown in Fig. 3 . The wind tunnel has a test section with a usable length of 30 ft , and a cross sectional area of 6 x 6 ft^2. Damping screens, located in the 4:1 contraction area, yield a free stream turbulence level $\frac{\sqrt{u'^2}}{\bar{u}_\infty}$ of less than 2% . A turbulent boundary layer was created by a strip of 1/4 in. gravel 14 in. long preceded by a trip fence of 1/2 in. saw teeth. These obstructions were placed at the tunnel's entrance. The hill model, a 2 x 2 in. wedge shown in Fig. 4 , was placed on the floor 14 ft downstream from the wind tunnel entrance.

Wind speed in the low speed wind tunnel was controlled with an axial fan, with 16 blades, which is driven at constant speed by a 75 hp motor. The velocity range of the tunnel is about 5 to 75 fps and is adjusted by remotely setting the variable pitch blades of the fan. Experiments were carried out at speeds of 45 and 30 fps. The pressure gradient along the center line of the wind tunnel before the hill model was installed is approximately zero at 30 fps. No pressure corrections were made after the installation of the models, because of the small obstruction which the model offered to the flow. Static pressure along the floor was measured by means of pressure taps embedded along the center line of the wind tunnel floor. The arrangement of the pressure taps can be seen in Fig. 3 .

B. Carriage

Vertical velocity or pressure profiles are obtained by a pitot tube or a hot-wire probe mounted on a remotely controlled positioning carriage. Components comprising the positioning system are a 28 V. D. C. motor, a potentiometer, a screw drive, a probe holder, a guide bar and a control box which is used to control the speed and direction of the motor. The D. C. motor drives the screw drive, which in turn moves the probe up and down. A probe is attached to the guide bar by means of probe holder which allows the probe to be moved a distance of 19 inches. A potentiometer is fixed on the

probe holder and geared to the guide bar. As the probe holder moves, a voltage drop corresponding to the distance travelled by the probe holder is produced across the potentiometer. This voltage is then transmitted to the x-axis of a X-Y plotter to give the position of the pitot tube.

C. Pitot Tube, X-Y Plotter, and Electronic Manometer

A pitot tube was used to measure mean flow velocity. The hot-wire anenometer, which will be discussed later, is used to measure the fluctuating components of velocity. Outside diameter of the pitot tube was 3/16 in. Plastic tubing was used to connect the pitot tube to a Transonic Equibar Type 120 electronic manometer, which has 8 ranges of pressure from 0.01 mm Hg to 30 mm Hg with a dc-output of 30 mv for each full scale reading. The electric manometer can detect pressure changes of 0.0002 mm Hg. Output of the electronic manometer was transmitted to the y-axis of a X-Y plotter, Moseley Type 135 . A voltage corresponding to the position of pitot tube was applied to the x-axis of the X-Y plotter. In this manner it was possible to plot out a continuous profile of the dynamic pressure or static pressure directly.

D. Mean Velocity Measurement

Mean velocity was measured with a pitot tube, which was mounted on the carriage. The free stream velocity was set at 45 and 30 fps. It was measured by placing the pitot tube 2 ft above the floor, upstream of the hill model. Vertical velocity profiles were measured from the floor to a height of 19 inches and from the model's crest to a distance of 60 inches downstream. Measurements were taken at various stations behind the model along the tunnel's center line. Air flow two-dimensionality was verified by velocity profiles taken at a few stations located on either side of the center line. These profiles were within one percent agreement as shown in Fig. 5 . Air temperatures and barometric pressure were also recorded during test runs.

The mean velocity measured with a pitot tube is calculated from the corresponding reading of the transonic manometer from the relation $\bar{u} = 2.36\sqrt{\frac{h}{\rho}}$. h is the transonic reading (in mm Hg) corresponding to the dynamic head, ρ is the density of air (in $\frac{lb - sec^2}{ft^4}$) and $\bar{u}$ is the velocity (in fps) .

A dynamic pressure is defined as the difference of the total pressure and the static pressure at the same point. However, for the pitot tube used, the total pressure and the static pressure are

not measured at the same point, but at points one-inch apart as shown in Fig. 6. If H_1, represents the total pressure at point 1, and if $\bar{p}_1$ and $\bar{p}_2$ represent the static pressure at point 1 and point 2 respectively, then the velocity at point 1, in terms of dynamic pressure should be:

$$\frac{1}{2}\rho\,\bar{u}^2 = H_1 - \bar{p}_1$$

However, the dynamic pressure measured with the pitot tube is

$$\frac{1}{2}\rho\,\bar{u}_m^2 = H_1 - \bar{p}_2$$

where $\bar{u}_m$ corresponding to the velocity measured with the pitot tube. The theoretical value and the measured value can be related as

$$\frac{1}{2}\rho\,\bar{u}^2 = H_1 - \bar{p}_2 + \bar{p}_2 - \bar{p}_1$$

$$= \frac{1}{2}\rho\,\bar{u}_m^2 + \left(\frac{\partial \bar{p}}{\partial x}\right)_1 \Delta x$$

The error of velocity due to pitot tube measurement is

$$\frac{\Delta \bar{u}}{\bar{u}} = \frac{\bar{u} - \bar{u}_m}{\bar{u}} = 1 - \frac{\bar{u}_m}{\bar{u}}$$

$$\frac{\bar{u}_m}{\bar{u}} = \left\{1 + \frac{\left(\frac{\partial \bar{p}}{\partial x}\right)_1 \Delta x}{\frac{1}{2}\rho \bar{u}_m^2}\right\}^{-\frac{1}{2}} = 1 - \frac{1}{2}\frac{\left(\frac{\partial \bar{p}}{\partial x}\right)_1 \Delta x}{\frac{1}{2}\rho \bar{u}_m^2}$$

$$\frac{\Delta \bar{u}}{\bar{u}} = \frac{1}{2}\frac{\left(\frac{\partial \bar{p}}{\partial x}\right)_1 \Delta x}{\frac{1}{2}\rho \bar{u}_m^2}$$

If the dynamic pressure is expressed in terms of the pressure transducer reading h, then the error takes the form

$$\frac{\Delta \bar{u}}{\bar{u}} = \frac{1}{2}\frac{\bar{p}_2 - \bar{p}_1}{\gamma h} \qquad (4\text{-}1)$$

where γ is the specific weight of air, and $\left(\frac{\partial \bar{p}}{\partial x}\right)_1 \Delta x$ is approximated by the pressure difference, i.e., $\left(\frac{\partial \bar{p}}{\partial x}\right)_1 \Delta x = \bar{p}_2 - \bar{p}_1$. If there is no pressure gradient in the x-direction, the pitot tube gives the true value of velocity. Further, if the difference of pressure $\Delta \bar{p}$ is small when compared with pitot tube reading h, the error would be very small and the velocity calculated directly from pitot tube reading is still within the accuracy required. In this investigation, the maximum error of velocity with the free stream velocity as reference is within 1.5%, so no effort was made to correct the pitot tube readings.

Liepmann and Laufer (9) have used both pitot tube and the hot-wire to measure the same mean velocity distribution separately, to see if there was any discrepancy existing between the results. They found both methods gave satisfactory agreement.

E. Static Pressure Measurement

Only the static hole of the pitot tube was used when measuring static pressure. Measuring instruments (seen in Fig. 7) were arranged in the same manner as for the measurements of the velocity measuring device, except that another pitot tube was used to give the static reference pressure. Throughout the experiment, the reference pitot tube was fastened to a slender bar located upstream from the hill model. The ba was suspended from the tunnel's ceiling and extended approximately 20 in. into the ambient stream. Static pressures were measured around the hill, along the center line of the floor. Pressures around the hill were measured by means of $\frac{1}{16}$ in. pressure taps around the model. (see Fig. 4) Static pressures along the floor were measured through pressure taps embedded in the floor. These pressure taps were connected successively through plastic tubing to the electronic manometer, where they were measured against the reference static pressure. Vertical static pressure distributions were measured in the same way as the mean velocity profiles, except that only the static hole

was used. Some fluctuation of static pressure was observed throughout the measurements. The largest amounts of fluctuation were found in the mixing region.

F. Turbulent Measurement

Turbulent quantities $\overline{u'^2}$, $\overline{u'v'}$ and $\overline{v'^2}$ were evaluated by using a constant temperature hot-wire anemometer. The fluctuating velocity component in the main stream direction $\overline{u'^2}$ was measured with a single wire probe. A cross wire was used in place of the single probe when measuring $\overline{u'v'}$ and $\overline{v'^2}$. Turbulent quantities were measured with the probe mounted on the positioning carriage. A platinum wire; which had a diameter of 0.0001 in. , a length of 0.1 in. and a cold resistance of approximately 5 ohms; was used as a sensor. This wire was mounted on a hot-wire probe made by DISA Company. The hot-wire probe was operated by a constant temperature type servo amplifier, Hubbard 3A , from which the A.C. output was fed into a true rms-meter, Type BRUEL and KJAER 2409 . This instrument had been modified to give an output voltage proportional to the meter reading. Output voltage from the rms-meter and the voltage proportional to the probe position were then applied to the two axes of an X-Y plotter, thus yielding continuous turbulent profiles. Instrument arrangement is shown in Fig. 8 . The output voltage of the Hubbard amplifier is

a linear function of velocity. From measurements with pitot tube and hot-wire, the free stream velocity is calibrated against the output reading of the hot-wire anemometer. A straight line calibration curve was obtained. Fig. 9 gives an example of this calibration curve. With the slope of the calibration curve determined, the turbulent quantities are obtained by conversion from the reading of the plotted profiles.

Turbulent velocity measurement made with a hot-wire anemometer are based on the principle that the heat loss per unit time is equal to the heat generated per unit time by an electric current passing through the wire. Heat loss is generally heat conduction, radiation, free and forced convection. In practice the effects of radiation and free convection are negligible. By King's law, the empirical relation between the heat loss and the mass flow can be written as

$$\frac{I^2 R_w}{R_w - R_a} = B + D\sqrt{u} \qquad (4\text{-}2)$$

Where R_w is the wire resistance while in operation, R_a is the wire resistance at air temperature and B and D are constants.

For constant temperature operation, the resistance is kept constant, the fluctuation of the velocity component will give rise to a fluctuation of heating current. If fluctuations of velocity and

current are both small compared with the mean values, then

$$\frac{2 I R_w}{R_w - R_a} dI = \frac{D}{2\sqrt{\bar{u}}} du$$

$$dI = I'$$

$$du = u'$$

The relation between the fluctuation of velocity and that of current is then determined as

$$I' = Su' \tag{4-3}$$

where S is the sensitivity of the hot-wire anemometer. In the instrument used, Hubbard Type 3A , the current (in milliampere) is passing through a resistor of 50, 000 ohms, across which the output voltage is measured. The output voltage e' (in volts) is then related to the fluctuating current through

$$e' = 50 I' \tag{4-4}$$

and to the fluctuating velocity

$$\frac{e'}{50} = I' = Su'$$

Therefore $$\overline{u'^2} = \left| \frac{A}{50} \right|^2 \overline{e'^2} \tag{4-5}$$

where $\overline{e'^2}$ is the mean square reading of the voltage output, and $A = \frac{1}{S} = \frac{du}{dI}$. The inverse of the sensitivity S is defined as the calibration constant A , which is obtained from the calibration curve of the mean velocity plotted against the mean current. A linearing circuit designed into the instrument is responsible for the straight line calibration curve in Fig. 9 . A is then determined by measuring the slope of the calibration curve. As a result, the turbulent quantities $\overline{u'^2}$ can be obtained from Eq. (4-5) .

Turbulent quantities $\overline{u'v'}$ and $\overline{v'^2}$ were measured with a cross wire probe. The two wires comprising this probe were inclined at angles α and β to the main stream direction as indicated in Fig. 10 . For this wire arrangement, the relations between fluctuations of currents and of velocities become

$$A_1 I'_1 = u' \cos\alpha + v' \sin\alpha \qquad \text{for wire 1}$$

$$A_2 I'_2 = u' \cos\beta - v' \sin\beta \qquad \text{for wire 2}$$

Square and then take the time-average

$$\left(\frac{A_1}{50}\right)^2 \overline{e'^2_1} = \overline{u'^2} \cos^2\alpha + 2\overline{u'v'} \sin\alpha \cos\alpha + \overline{v'^2} \sin^2\alpha \qquad (4\text{-}6)$$

$$\left(\frac{A_2}{50}\right)^2 \overline{e_2'^2} = \overline{u'^2}\cos^2\beta - 2\,\overline{u'v'}\sin\beta\cos\beta + \overline{v'^2}\sin^2\beta \tag{4-7}$$

For the experiments presented in this study the angles were $\alpha = 38^0$, $\beta = 43^0$ and the calibration curve was given by the equation $\bar{u} = 43\ I : 7.5$, where $A_1 = A_2 = 43$. With these values, subtracting Eq. (4-7) from Eq. (4-6) yields

$$\left(\frac{43}{50}\right)^2 (\overline{e_1'^2} - \overline{e_2'^2}) = \overline{u'^2}(\cos^2\alpha - \cos^2\beta) + \overline{u'v'}(\sin 2\alpha + \sin 2\beta) + \overline{v'^2}(\sin^2\alpha - \sin^2\beta)$$

which yields $$\overline{u'v'} = 0.376\,(\overline{e_1'^2} - \overline{e_2'^2}) \tag{4-8}$$

Further, adding Eq. (4-6) and Eq. (4-7) leads to

$$\left(\frac{43}{50}\right)^2 (\overline{e_1'^2} + \overline{e_2'^2}) = \overline{u'^2}(\cos^2\alpha + \cos^2\beta) + \overline{u'v'}(\sin 2\alpha - \sin 2\beta) + \overline{v'^2}(\sin^2\alpha + \sin^2\beta)$$

or $$\overline{v'^2} = 0.377\,(\overline{e_1'^2} + \overline{e_2'^2}) - 1.37\,\overline{u'^2} \tag{4-9}$$

From Eq. (4-8) and Eq. (4-9), $\overline{v'^2}$ and $\overline{u'v'}$ can be calculated.

G. Measurement of Reattachment Point

A special technique was developed (16) to measure the reattachment point. Two hot wires of exactly the same length and resistance were placed parallel and as close as possible without touching in the separated region. Each one was operated by one channel of the two-channel Hubbard hot-wire anemometer amplifier. The outputs of the hot-wire amplifiers were fed into a special discriminating circuit, designed by Mr. Calvin Finn. This discriminating circuit provides a train of 100,000 pulses per second as long as the input to one preset discriminator channel (channel A) is larger than the input to the other channel (channel B) . If the input to channel B is larger then no signal is generated by the circuit.

Now if the two-wire probe is placed at some suitable distance above the floor with the plane through the axes of the wires parallel to the floor, then, when the flow velocity is parallel to the floor, the downstream wire is in the wake of the upstream wire and consequently does not get cooled as much as the upstream wire. Under these conditions the feedback amplifier would give a larger current output for the wire located upstream than for the downstream wire. If the signals from the two wires are fed into the discriminating circuit it yields an output which when transferred to a pulse counter (Hewlett Packard Type 522) , indicates the percent of time one wire

yields a larger signal than the other. The reattachment point was defined as that location where the individual direction of flow is equal in both directions (a 50% reading on the discriminator) . The reattachment point was thus found at 25. 5 in. downstream from the hill when the free stream velocity was 45 fps. The equipment is shown in Fig. 11 .

Chapter V

ANALYSIS AND DISCUSSION

The flow along the separation region behind a hill is similar to a half-jet mixing with the ambient fluid at rest. Therefore, the velocity profiles along the separation region can be described by Equation (3-15) which was obtained for a half-jet

$$\frac{\bar{u}}{\bar{u}_1} = \frac{1}{2}(1 + \text{erf}\,\xi)$$

where $\xi = \sigma \frac{y}{x}$ and σ is a constant.

In this equation, x and y are the coordinates of an intrinsic coordinate system in the flow. The relation between the intrinsic coordinate and the reference coordinate system can be derived from Eq. (3-15), as will be discussed below.

A. Free Stream Velocity

When air flows over the hill, a separation bubble forms directly behind the hill. Inside the bubble there exists a vortex region where the velocity is very small and may be considered as being almost equal to zero. Between the bubble and the free stream

there is a mixing layer across which the velocity increases rapidly from zero to the free stream velocity. Influence of the hill causes the velocity in the separation region above the bubble to rise to a peak value near the crest of the hill, and then decrease gradually over a distance to reach an equilibrium value. The amount of this velocity decrease is about 5% to 8% of the maximum value. Maximum velocity is then defined as free stream velocity $\bar{u}_1$. Mean velocity profiles behind the hill are shown in Fig. 12 . The velocities near the floor are left out because there is a reversed flow near the floor, which is hard to measure correctly with the pitot tube. The locus of the points which correspond to the maximum velocity is then defined as the upper boundary of the half-jet mixing region, which is a small gradient curve seen in Fig. 13 . With the free stream velocity determined, the ratio of local velocity to the free stream velocity is only a function of local position as described by Eq. (3-15) .

Figure 14 presents the velocity variation along the upper boundary where $\frac{\bar{u}}{u_1} = 1$, and along the central velocity line $\frac{\bar{u}}{u_1} = \frac{1}{2}$, that is, the jet-axis. The velocity was made dimensionless by dividing by the corresponding velocity at the crest of the hill. A small variation of the half-jet free stream velocity was observed along the distance downstream. At first, the velocity

increases, then it decreases and tends to approach a constant value downstream near the end of the separation region. The pressure gradient in the x-direction, which is implied in the variation of the free stream velocity, was shown by Sabin (20) as making only a small contribution to the turbulent shear stress. If the variation of free stream velocity is neglected, which means the pressure gradient in the x-direction is assumed to be zero, the analysis is simplified and the error introduced would not have a significant effect on the end results. This has been done in this analysis.

B. Transformation of Coordinates

An intrinsic coordinate system, x and y , is used in half-jet analysis, refer to Eq. (3-15) . Measurements use a fixed reference coordinate system. This system consists of X and Y-axis which originated at the front edge of the hill model. The X-axis appears along the floor with a positive downstream direction. The Y-axis is normal to the floor with a positive direction upward. The relation between the coordinate system can be obtained from Eq. (3-15) .

Location of the X-axis can be found from the experimental data according to the following procedure. If the velocity distribution

is given by

$$\frac{\bar{u}}{\bar{u}_1} = \frac{1}{2}(1 + \text{erf}\,\xi)$$

where $\xi = \sigma \frac{y}{x}$

then it follows that

if $y = 0$ then $\xi = 0$

and the velocity ratio becomes

$$\frac{\bar{u}}{\bar{u}_1} = \frac{1}{2}$$

This means that the x-axis coincides with central velocity line where $\frac{\bar{u}}{\bar{u}_1} = \frac{1}{2}$. Since the free stream velocity $\bar{u}_1$ has been determined as the maximum velocity, the x-axis can be found easily from the measured velocity profile by locating the points where $\frac{\bar{u}}{\bar{u}_1} = \frac{1}{2}$. Fig. 13 illustrates an x-axis obtained in the foregoing manner. This x-axis was observed to curve up from the crest of the hill and soon approach a straight line parallel to the floor. The angle between the y-axis and the Y-axis due to the curvature of the x-axis is so small as to be negligible. Therefore, the y-axis is assumed to coincide approximately with the Y-axis. Let Y_c

represent the Y-coordinate of the central velocity line, namely, the x-axis, then a relation between y and Y can be established as $y = Y - Y_c$ shown in Fig. 15 .

The initial curvature section of the x-axis is rather short. Thus, the distance along the x-axis is approximated by the distance along the X-axis, i.e., by the distance parallel to the floor. The error introduced by such an approximation is small at large distance. Finally, the transformation of the intrinsic coordinate system into the fixed reference system is given by

$$y = Y - Y_c \tag{5-1}$$

$$x = X$$

At this point, it is possible to compare the measured value with the theoretical value obtained by Eq. (3-15) , if there is a suitable value for similarity parameter σ .

C Half-Jet Boundary

Theoretically, the velocity profiles given by Eq. (3-15) result in a velocity equal to the free stream velocity at an infinite distance from the x-axis. Therefore, the boundary line is usually defined at $\frac{\bar{u}}{\bar{u}_1} = 0.99$ to avoid this difficulty. In this investigation, the upper boundary is defined as the maximum velocity point in the

profile. The upper boundary is presented in Fig. 13 , which does not appear as a straight line but as a curve. This curvature is large directly behind the hill, but at a short distance downstream the curvature decreases to the point that it may be approximated by a straight line. This curved boundary is in contradiction to the classical half-jet studies. However, in an investigation of turbulent, incompressible, symmetrical mixing of two parallel streams, T. P. Torda also found a curved boundary which he attributed to the initial boundary layer thickness upstream of the trailing edge of the flat plate. In addition to the effect of initial boundary layer thickness, the obstruction of the hill in the flow might contribute to the curvature of the half-jet. The hill extended from the floor into the flow. Therefore, the flow upstream, below the height of the hill, was forced to rise as it approached the hill. As a consequence, a velocity component normal to the mean stream direction appeared near the hill. The half-jet mixing region which was slightly displaced by this vertical velocity component will have curved appearance. This normal velocity died out further downstream so that the curvature reduced correspondingly.

The lower boundary for half-jet mixing, which lies within the vortex region in the separation bubble, was not well defined. An attempt was made to define this lower boundary by a constant velocity

ratio line $\frac{\bar{u}}{\bar{u}_1} = 0.1$, but the data are too irregular to define a regular curve. There is a reversal of flow within the separation bubble caused by the entrainment of air into the jet region. The pitot tube was not oriented to measure this reverse velocity. The large scatters in the reading may be due to the inability of pitot tube to read accurately the velocity in the bubble.

D. Spread of Width

In view of the difficulty in defining the lower boundary of a half-jet mixing region as mentioned before, the mixing region is divided into two zones: Zone I and Zone II . Zone I, as seen in Fig. 16, is the region above the x-axis up to the upper boundary line where $\frac{\bar{u}}{\bar{u}_1} = 1$; and Zone II is the region below the x-axis. Both the upper boundary and the x-axis of the half-jet are curved rather than linear. The distance between the two lines, which is the width of Zone I , was observed to vary approximately linearly over a distance of 4 to 20 inches downstream from the model hill. Further downstream, it tends to approach an asymptotic value. This linear variation of the width with distance is in agreement with half-jet theory.

The spread of the width of Zone I is plotted in Fig. 17. The width of Zone II is not shown because the low boundary of the jet is

poorly defined. The spread of the width of the mixing region is found to decrease with an increase of free stream velocity. The width when free stream velocity is 30 fps is bigger than when the velocity is 45 fps.

E. Proximity of Floor

In half-jet analysis, it is supposed that no solid boundary exists in the neighborhood of the mixing region. However, in this study of separation flow, there is a floor behind the model hill. The effect due to the proximity of the floor is felt in the region near the floor and will decrease with the distance from the floor.

Zone I is far enough away from the floor that the effect of the floor is so slight as to be unnoticeable, and the separation flow in this region develops as a half-jet. In Zone II , which is below the jet-axis and near the floor, the influence of the floor on the flow is stronger. This influence is found from measured velocity data deviation from analytical results. The floor also restricts the width of Zone II and as a result Zone II is narrower than Zone I .

The most important floor effect is the formation of a separation bubble which adds complexity to the problem. Jet flow near the outer edge of the bubble entrains the fluid from the bubble by the action of the shearing stress, thus causing the pressure inside the bubble to decrease. This decrease in pressure forces the lower part

of half-jet toward the floor. The bubble also causes the half-jet mixing region to spread vertically as distance increases. As a result of this, there is a point downstream from the hill where the flow reattaches to the floor with an amount of the flow reversed back into the bubble. Mass conservation requires that the amount of fluid entrained from the bubble should be balanced by the amount of the reversed flow at reattachment. The air in the separation bubble is thus induced into a circulatory motion to form an eddy vortex. Because it is hard to use pitot tube to measure the reversed flow in the bubble, the velocities near the floor are left out in Fig. 5 and Figure 12 . However, the pitot tube is capable of measuring the static pressure in the reversed flow, and the pressure inside the bubble is found lower than the pressure outside.

F. Pressure Gradient and Curvature

Pressure gradients are found both in the main stream direction and in the transverse direction. Fig. 18 shows the variation of static pressure along the constant velocity ratio lines and Fig. 19 shows the variation of static pressure at constant heights above the floor, downstream of the hill. The development of static pressure distribution downstream of the hill is shown in Fig. 20 . Near reattachment the static pressure was observed to increase over a large horizontal distance. Below the jet-axis the pressure is

nearly uniform. Most of the variation of static pressure from the pressure in the separation bubble to the pressure in the external free stream takes place in the region above the jet axis to the outer jet boundary, that is, Zone I . The pressure difference across Zone I becomes smaller and smaller further downstream. The horizontal pressure gradient has been found by Sabin (20) to have only a slight effect on the turbulent mixing mechanism and consequently was neglected in this investigation. However, transverse pressure gradient across the mixing region induces a curvature in the separated flow.

The curvature can be seen in the equation in the cylinder coordinates (5) . Assume $\bar{u}$ is parallel to the streamlines, so that $\bar{v} = 0$. Then the equation of motion along a streamline is

$$\frac{\bar{u}^2}{r} = \frac{1}{\rho}\frac{\partial \bar{p}}{\partial r} + \frac{\partial \overline{v'^2}}{\partial r} + \frac{\overline{v'^2}}{r} + \frac{1}{r}\frac{\partial \overline{u'v'}}{\partial \theta} - \frac{\overline{u'^2}}{r} \qquad (5\text{-}2)$$

in which the viscous stress components, which are very small in free turbulent shear flow, are omitted. Eq. (5-2) may be rearranged as

$$\frac{\bar{u}^2}{r}\left[1 + \frac{\overline{u'^2}}{\bar{u}^2} - \frac{\overline{v'^2}}{\bar{u}^2} - \frac{1}{\bar{u}^2}\cdot\frac{\partial(\overline{u'v'})}{\partial \theta}\right] = \frac{1}{\rho}\frac{\partial \bar{p}}{\partial r} + \frac{\partial \overline{v'^2}}{\partial r}$$

Assume the streamlines in the separated flow are parallel to each other, so the radius of streamline R is constant at each cross

section, i.e., R is not a function of r . Integrating the above equation over r ,

$$\frac{1}{R}\int \rho\bar{u}^2 \left[1 + \frac{\overline{u'^2}}{\bar{u}^2} - \frac{\overline{v'^2}}{\bar{u}^2} - \frac{1}{\bar{u}^2} \cdot \frac{\partial \overline{u'v'}}{\partial \theta} \right] dr =$$

$$= \int \left[\frac{\partial \bar{p}}{\partial r} + \rho \frac{\partial \overline{v'^2}}{\partial r} \right] dr$$

As shown in Fig. 21 , the turbulent quantities $\frac{\overline{u'^2}}{\bar{u}^2}$, $\frac{\overline{v'^2}}{\bar{u}^2}$, $\frac{\overline{u'v'}}{\bar{u}^2}$ are very small. Their integral are much smaller when compared with the integral of the term $\bar{u}^2$, so these turbulent quantities are neglected. It yields

$$\frac{1}{R}\int \rho\bar{u}^2 \, dr = \int \frac{\partial \bar{p}}{\partial r} dr + \int \rho \frac{\partial \overline{v'^2}}{\partial r} dr \qquad (5\text{-}3)$$

The radial coordinate can be approximated by the y-coordinate. The integral is taken from the jet-axis to the outer jet boundary. Then

$$\frac{1}{R}\int_0^{y_1} \rho\bar{u}^2 \, dy = \int_0^{y_1} \frac{\partial \bar{p}}{\partial y} dy + \rho \int_0^{y_1} \frac{\partial \overline{v'^2}}{\partial y} dy$$

$$= (\bar{p} + \rho\overline{v'^2})_{y = y_1} - (\bar{p} + \rho\overline{v'^2})_{y = 0}$$

$$= \Delta\bar{p} + \rho \, \Delta\overline{v'^2}$$

$$\approx \Delta\bar{p}$$

Since $\rho \Delta\overline{v'^2}$ is much smaller than $\Delta\bar{p}$ as can be seen in Fig. 21, it is neglected . . The radius of curvature is thus obtained

$$R = \frac{\rho \int_0^{y_1} \bar{u}^2 \, dy}{\Delta\bar{p}} \qquad (5\text{-}4)$$

The pressure difference $\Delta\bar{p}$ decreases with x, so the radius of curvature R increases with x as shown in Fig. 22 . This relation indicates how the separated flow is bent by the action of the transverse pressure gradient.

G. Similarity Parameter

The emperical similarity parameter σ is usually chosen when fitting velocity data to theory. Previous investigators have found various values of σ . For instance, Liepmann and Laufer (9) , in their experiments of a two-dimensional mixing layer, found that the best value for presenting experimental results according to Tollmien's theory was 12 , but by Gortler's theory $\sigma = 11$ gave better agreements. Reichardt (18) found that $\sigma = 13.5$ for the half-jet case and $\sigma = 7.67$ for the two-dimensional jet when Gortler's theory was employed. Sawyer (21 chose $\sigma = 15$ in his analysis of a two-dimensional jet issuing parallel to a flat plate.

The non-dimensional velocity profiles are given by Eq. (3-15)

$$\frac{\bar{u}}{\bar{u}_1} = \frac{1}{2}(1 + \text{erf}\,\xi)$$

In this equation the central velocity line where $\frac{\bar{u}}{\bar{u}_1} = \frac{1}{2}$, is defined on the x-axis where $y = 0$ implying that $\xi = 0$. A suitable choice of two velocities will make it possible to calculate the similarity parameter σ. The following method is used in this study to find the first approximate value of σ.

Let Y_α denote the Y coordinate of the points where $\frac{h}{h_1} = \alpha$. h is the reading of the pressure manometer which corresponds to the dynamic head, and subscript 1 refers to the free stream. Similarly Y_β corresponds to $\frac{h}{h_1} = \beta$.

Equation $\frac{\bar{u}}{\bar{u}_1} = \frac{1}{2}(1 + \text{erf}\,\xi)$

gives $$\text{erf}\,\xi = 2\frac{\bar{u}}{\bar{u}_1} - 1 = 2\sqrt{\frac{h}{h_1}} - 1$$

At any station x, $\frac{h}{h_1} = \alpha$ gives a value of ξ_α and $\frac{h}{h_1} = \beta$ gives a value of ξ_β.

By definition

$$\xi_\alpha = \sigma \frac{y_\alpha}{x} = \sigma \frac{Y_\alpha - Y_c}{X}$$

$$\xi_\beta = \sigma \frac{y_\beta}{x} = \sigma \frac{Y_\beta - Y_c}{X}$$

As σ is assumed constant across the mixing region, the similarity parameter might be obtained by

$$\xi_\alpha - \xi_\beta = \Delta\xi = \sigma \frac{Y_\alpha - Y_\beta}{X} = \sigma \frac{\Delta Y}{X}$$

Therefore

$$\sigma = \frac{\Delta\xi}{\Delta Y} X = \frac{\xi_\alpha - \xi_\beta}{Y_\alpha - Y_\beta} X . \qquad (5\text{-}5)$$

ξ_α and ξ_β are derived theoretically from the equation while Y_α and Y_β are read directly from the measurements. This method makes it possible to determine σ from the empirical data. In this thesis analysis is based on $\alpha = 0.9$, $\beta = 0.1$. Correspondingly, $\xi_{0.9} = 1.15$ and $\xi_{0.1} = -0.345$. $Y_{0.9}$ and $Y_{0.1}$ were read at each station. However, this approximate value of σ did not yield the best agreement between theory and measurement. It became necessary to make few adjustments to improve the agreements. The velocity profile based on the measurements were compared with the

theoretical profile given by Eq. (3-15) in Fig. 23 . Results of the comparison were in agreement, which implied that the velocity profile in the separation region has the same characteristic as the half-jet mixing layer. However, it was discovered that the similarity parameter σ increases with distance rather than remaining constant for all value of x . σ was plotted against x on a logarithmic paper as shown in Fig. 24 . This plot showed that most of the points were scattered around a straight line, except those very near the hill and those approaching the reattachment point. A slope of approximate 0.5 was found from the plot which meant that σ increases with $\sqrt{x}$. This contradicts the assumption leading to Equation (3-15) in which σ was assumed to be independent of x .

Despite this discrepancy, if σ is considered as a pure empirical factor without regard to its physical meaning, Eq. (3-15) still gives a successful description of the velocity distribution along the separation region behind a two-dimensional hill. However, further insight into the character of the similarity parameter σ can be seen by considering the effects of the initial boundary layer thickness and curvature. With the consideration of the initial boundary layer thickness as implied in Eq. (3-17) , Kirk's approximation of a displaced asymptotic profile will modify σ into σ_o.

$$\sigma_o = \sigma \left(1 + \frac{x_o}{x}\right)$$

The displacement of the virtual origin x can be obtained from Fig. 17 . This can be done by extending the straight line that represents the linear spread of Zone I width upstream. The intersection of this line with the x-axis is then the virtual origin where it is assumed the half-jet starts to develop. The distance from the crest of the hill model to the virtual origin was measured and was found to be x_o = 20 inches. Fig. 25 shows the similarity parameter σ_o obtained by this method. Although σ_o is still not a constant, its variation with distance is much smaller and a constant value is approached.

The variation of σ_o with x might be attributed to the curvature of the separated flow which is due to the transverse pressure gradient. This effect is implied in Eq. (3-20) .

$$\sigma_o = \frac{\sigma^*}{\sqrt{1 - mQ}}$$

where $Q = \frac{\bar{u}}{R} \cdot \frac{1}{\frac{\partial \bar{u}}{\partial y}}$

from $\frac{\bar{u}}{\bar{u}_1} = \frac{1}{2}(1 + \operatorname{erf} \xi)$

it yields $\frac{\partial \bar{u}}{\partial y} = \frac{\bar{u}_1 \sigma}{\sqrt{\pi} x} e^{-\xi^2}$

then $$Q = \frac{\bar{u}}{\bar{u}_1} \frac{x\sqrt{\pi}}{R\sigma} \cdot e^{\xi^2} \qquad (5\text{-}6)$$

It is obvious that the value of Q varies with y. It was decided that the mean value of Q could represent the characteristic of the whole region across the separated flow. This value was obtained as follows:

$$Q_{mean} = \frac{\int_{y_{0.1}}^{y_{0.9}} Q\, dy}{y_{0.9} - y_{0.1}}$$

$$= \frac{x}{R\sigma} \cdot \frac{\sqrt{\pi}}{2} \cdot \frac{1}{\xi_{0.9} - \xi_{0.1}} \int_{\xi_{0.1}}^{\xi_{0.9}} (1 + \operatorname{erf} \xi)\, e^{\xi^2}\, d\xi$$

where $y_{0.9}$ and $\xi_{0.9}$ denote the value of y and ξ respectively where $\frac{h}{h_1} = 0.9$, so is $y_{0.1}$ and $\xi_{0.1}$. The integration was carried out graphically from $\xi_{0.1} = -0.345$ to $\xi_{0.9} = 1.15$ it yields

$$Q_{mean} = 2\frac{x}{R\sigma} \qquad (5\text{-}7)$$

For zero curvature the similarity parameter $\sigma^* = 12$ was used The value of m can be then obtained from Eq. (3-21). Sawyer used $m = 5$ in his analysis of a two-dimensional jet. However, the value

of m found in this study is not a constant as it varies from 5 to 6 as shown in Fig. 26 . This indicates that a successful description of the effect of curvature on the turbulent mixing mechanism is necessary.

H. Velocity Distribution in Separated Flow

The primary purpose of this thesis is to investigate the velocity distribution in the separated flow behind a two-dimensional hill. The development of mean velocity distributions behind the hill can be seen in Fig. 12 . The velocity near the floor is not plotted out because it is difficult to measure the reverse velocity in the bubble with a pitot tube. The theoretical velocity profile for a half-jet is given by Eq. (3-15) , which is used to compare with the measured velocity profiles in the separated flow. From measurements, free stream velocity and the x-axis can be determined as described previously in this chapter. A suitable value for the similarity parameter σ is then chosen and the measured velocity profiles are plotted out non-dimensionally in Fig. 23 with $\frac{\bar{u}}{u_1}$ against ξ . Theoretical velocity profile is also plotted in the same figure. Deviations are observed in the lower part of Zone II . This deviation becomes larger near the floor which may be due to the presence of the separation bubble and the failure of pitot tube to measure velocity

correctly in the bubble. However, satisfactory agreement is found between the half-jet theory and the measurements over most of separation region, especially in Zone I .

Chapter VI

SUMMARY AND SUGGESTIONS

A. Summary

Velocity profiles in a turbulent separated flow of an incompressible fluid were investigated using the concept of free turbulence. The flow separated at the crest of a wedge shaped model hill and reattached itself to the floor downstream of the hill forming a separation bubble. Gortler's half-jet theory to the first order approximation is employed in the analysis of the separated flow. Analysis is simplified by neglecting the initial boundary layer thickness and by assuming that there is no pressure gradient in both the main stream and transverse direction. Satisfactory agreements between theory and experiments were found. The following results were obtained:

1. The velocity profiles in the separated flow over most region are successfully described by the half-jet theory; except those near the hill, reattachment point and the vortex region in the bubble.
2. Initially the jet boundary and jet axis are curved and

then approach to straight lines. The width between the two lines varies linearly with the distance.

3. A similarity parameter σ is used to relate the measurements and theoretical values. The parameter is not a constant but is proportional to the half-power of the distance from the crest of the model hill.
4. The curvature of the separated flow is induced by the action of the pressure gradient across the mixing region in the transverse direction. This transverse pressure gradient is large only in a short region immediately behind the hill. Further downstream the pressure gradient becomes so small that the curvature of the separated flow can be neglected.

Finally, the similarity parameter is modified by Kirk's approximation of displaced origin to include the effect of the initial boundary layer thickness. The effect of curvature on the similarity parameter is approximated by the first order theory of Sawyer. However, the results indicate that a better interpretation of the effect of curvature and a better definition of the radius of curvature are needed.

B. Suggestions for Further Study

It is recommended that further studies be made:

1. to measure the velocity inside the separation bubble. Since the pitot tube fails to give a reliable measurement of the reverse velocity in the bubble, an improved instrument will be needed for this purpose.
2. to find the streamlines in the flow field behind the hill. These were not obtained in this study because no measurement was made to read the reverse velocity in the bubble.
3. to determine the radius of curvature of the separated flow in a more logical way. In this study, the radius of curvature is assumed constant across the separated flow and this is a very rough assumption.
4. to investigate the entrainment of the fluid from the bubble by the separated flow and to find out its effect on the velocity profile in the separation region.
5. to include in the analysis of the separated flow the pressure gradients in both the x-direction and the y-direction.

6. to make a systematic study of the effects of the shape and of the size of the hill on the development of the velocity profiles in the separated flow.
7. to study the effect of the standing eddies appearing in front of the hill on the separated flow.

BIBLIOGRAPHY

BIBLIOGRAPHY

1. Chapman, A. J. and H. H. Korst, Free jet boundary with consideration of initial boundary layer. Proceedings of The Second U. S. National Congress of Applied Mechanics, p. 723-31, New York, The American Society of Mechanical Engineers, 1954.

2. Chapman, D. R., An analysis of base pressure of supersonic velocities and comparison with experiment. U. S. National Advisory Committee for Aeronautics, Report 1051, 1951, 23 p.

3. Federal Works Agency, Table of probability functions, vol. 1, New York Work Projects Administration for the City of New York, 1941, 306 p.

4. Forthmann, E., Turbulent jet expansion. U. S. National Advisory Committee for Aeronautics, Technical Memorandum 789, 1936. 18 p.

5. Hinze, J. O., Turbulence: An introduction to its mechanism and theory. New York, McGraw-Hill Book Company, 1959, 586 p.

6. Kirk, F. N., An approximate theory of base pressure in two-dimensional base flow at supersonic speeds. Great Britain Royal Aircraft Establishment, Technical Note Aero. 2377, 1959.

7. Korst, H. H., A theory for base pressure in transonic and supersonic flow. Journal of Applied Mechanics 23:593-600, 1956.

8. Kuethe, A. M., Investigations of the turbulent mixing regions formed by jets. Journal of Applied Mechanics 2:87-95, 1935.

9. Liepmann, H. W. and J. Laufer, Investigations of free turbulent mixing. U. S. National Advisory Committee for Aeronautics, Technical Note 1257, 1947, 68 p.

10. McDonald, H., Turbulent shear layer reattachment with special emphasis on the base pressure problem. The Aeronautical Quarterly 15:247-80, 1964.

11. McDonald, H., A study of the turbulent separated-flow region occurring at a compression corner in supersonic flow. Journal of Fluid Mechanics 22:481-505, 1965.

12. Millikan, C. B., A critical discussion of turbulent flow in channels and circular tubes. Proceedings of Fifth International Congress for Applied Mechanics, p. 386-392, Cambridge, 1938.

13. Mueller, T. J., H. H. Korst, and W. L. Chow, On the separation reattachment, and redevelopment of incompressible turbulent shear flow. Transactions of The American Society of Mechanical Engineers, Journal of Basic Engineering 86:221-26, 1964.

14. Pai, S. I., Fluid dynamics of jet. New York, Van Nostrand, 1954, 227 p.

15. Pai, S. I., Two-dimensional jet mixing of a compressible fluid. Journal of the Aeronautical Sciences 16:463-69, 1959.

16. Plate, E. J. and C. W. Lin, Velocity field downstream from a two-dimensional model hill. Part 1, Fort Collins, Colorado State University, February 1965, 75 p. (CER65EJP14, AD614067)

17. Plate, E. J. and V. A. Sandborn, An experimental study of turbulent boundary layer structure. Fort Collins, Colorado State University, December 1964, 49 p. (CER64EJP-VAS37, AD612168)

18. Reichardt, H., On new theory of free turbulence. Journal of Royal Aeronautical Society 47:167-76, 1943.

19. Roshko, A. and G. J. Thomke, Flow separation and reattachment behind a downstream-facing step. Douglas Report SM-43056-1, Douglas Missile and Space Systems Division, Santa Monica, Douglas Aircraft Company, Inc., California, 1964, 43 p.

20. Sabin, C. M., An analytical and experimental study of the plane, incompressible, turbulent free shear layer with arbitrary velocity ratio and pressure gradient. Palo Alto, Stanford University, October 1963, 122 p.
(Report MD9, AFOSR TN 5443, AD430120)

21. Sawyer, R. A., The flow due to a two-dimensional-jet issuing parallel to a flat plate. Journal of Fluid Mechanics 9:543-60, 1960.

22. Sawyer, R. A., Two-dimensional reattaching jet flows including the effects of curvature on entrainment. Journal of Fluid Mechanics 17:481-98, 1963.

23. Schlichting, Boundary layer theory. New York, McGraw-Hill Book Company, 1960, 647 p.

24. Squire, H. B., Reconsideration of the theory of free turbulence. Philosophical Magazine 39:1-20, 1948.

25. Squire, H. B. and J. Trouncer, Round jet in a general stream. Great Britain Aeronautical Research Council, Report and Memoranda 1974, 1944.

26. Tollmien, W., Calculation of turbulent expansion processes. U. S. National Advisory Committee for Aeronautics, Technical Memorandum 1085, 1945, 21 p.

27. Torda, T. P., W. O. Ackermann, and H. R. Burnette, Symmetric turbulent mixing of two parallel streams. Journal of Applied Mechanics 20:63-71, 1953.

28. Townsend, A. A., The structure of turbulent shear flow. London, Cambridge University Press, 1956, 315 p.

FIGURES

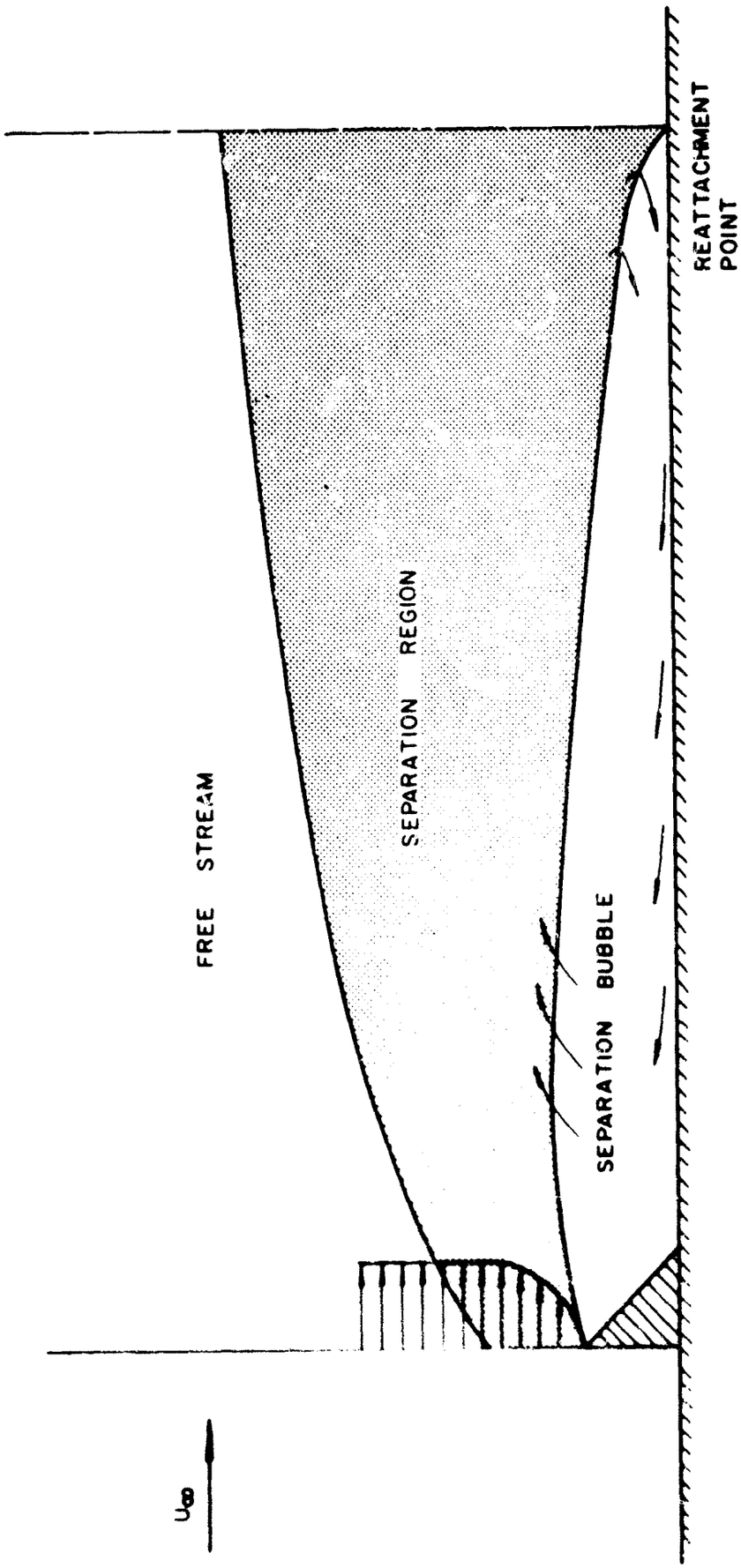

FIG. 1 FLOW FIELD BETWEEN HILL AND REATTACHMENT POINT.

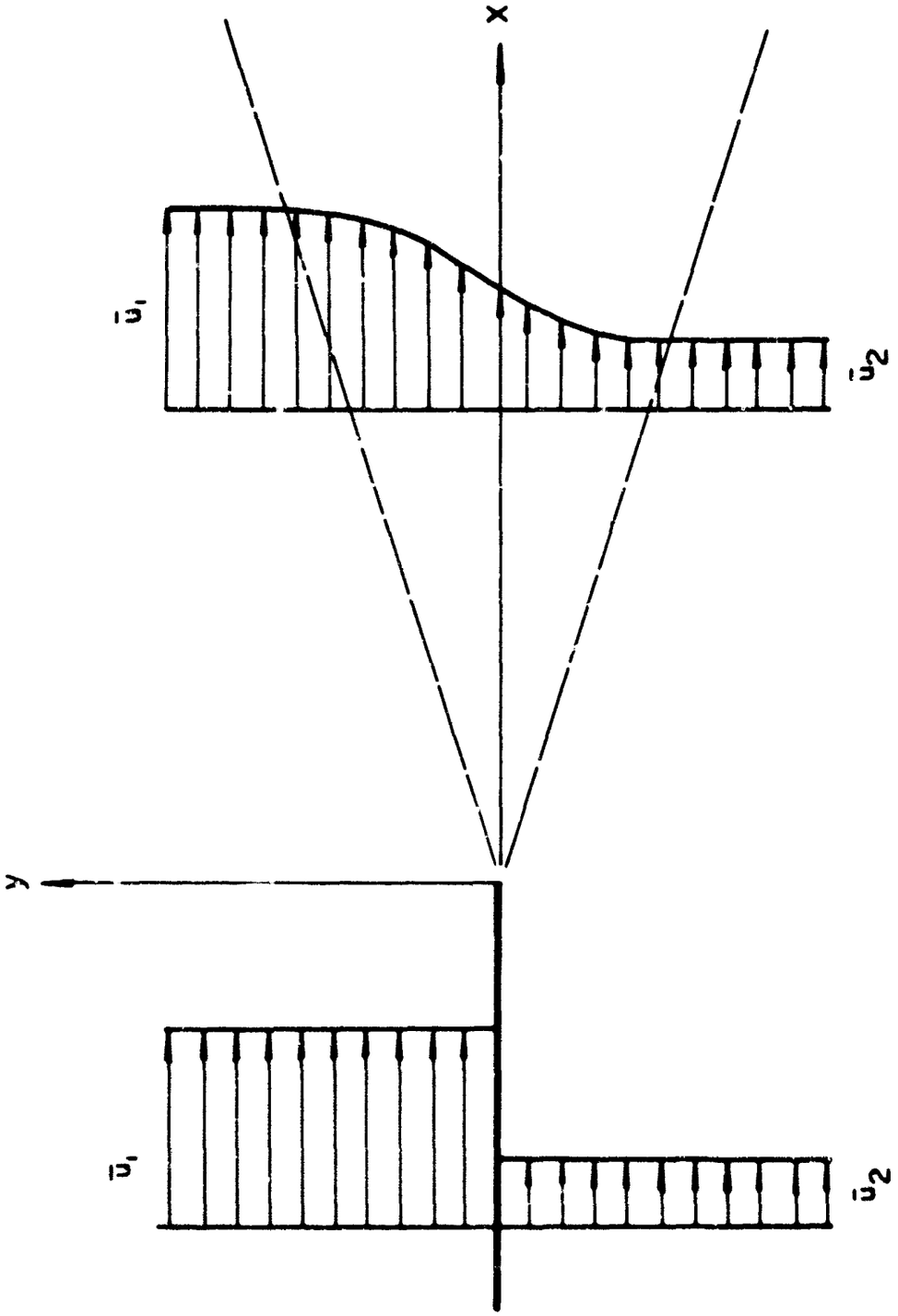

FIG. 2 HALF - JET

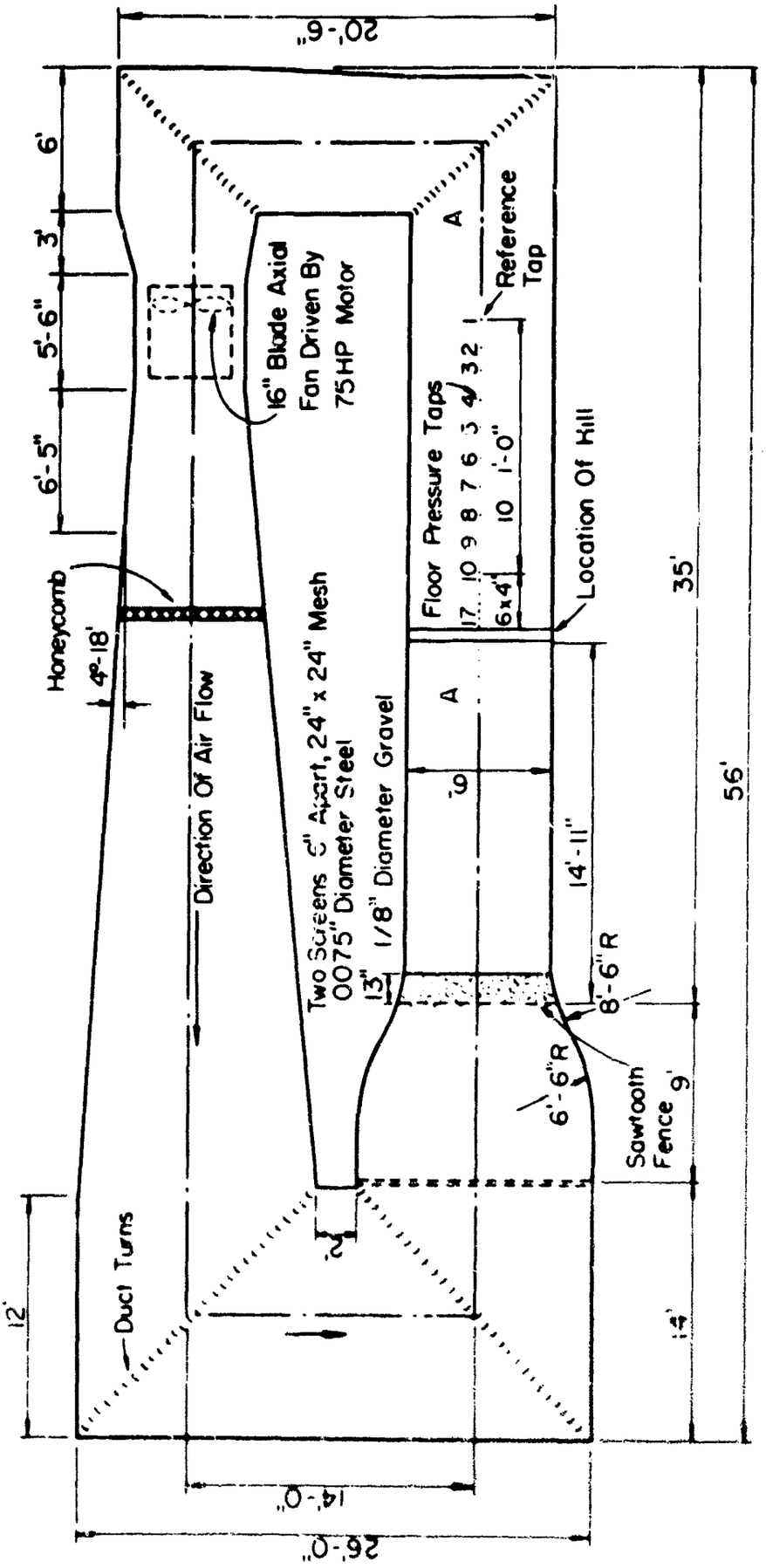

FIG. 3 SMALL WIND TUNNEL

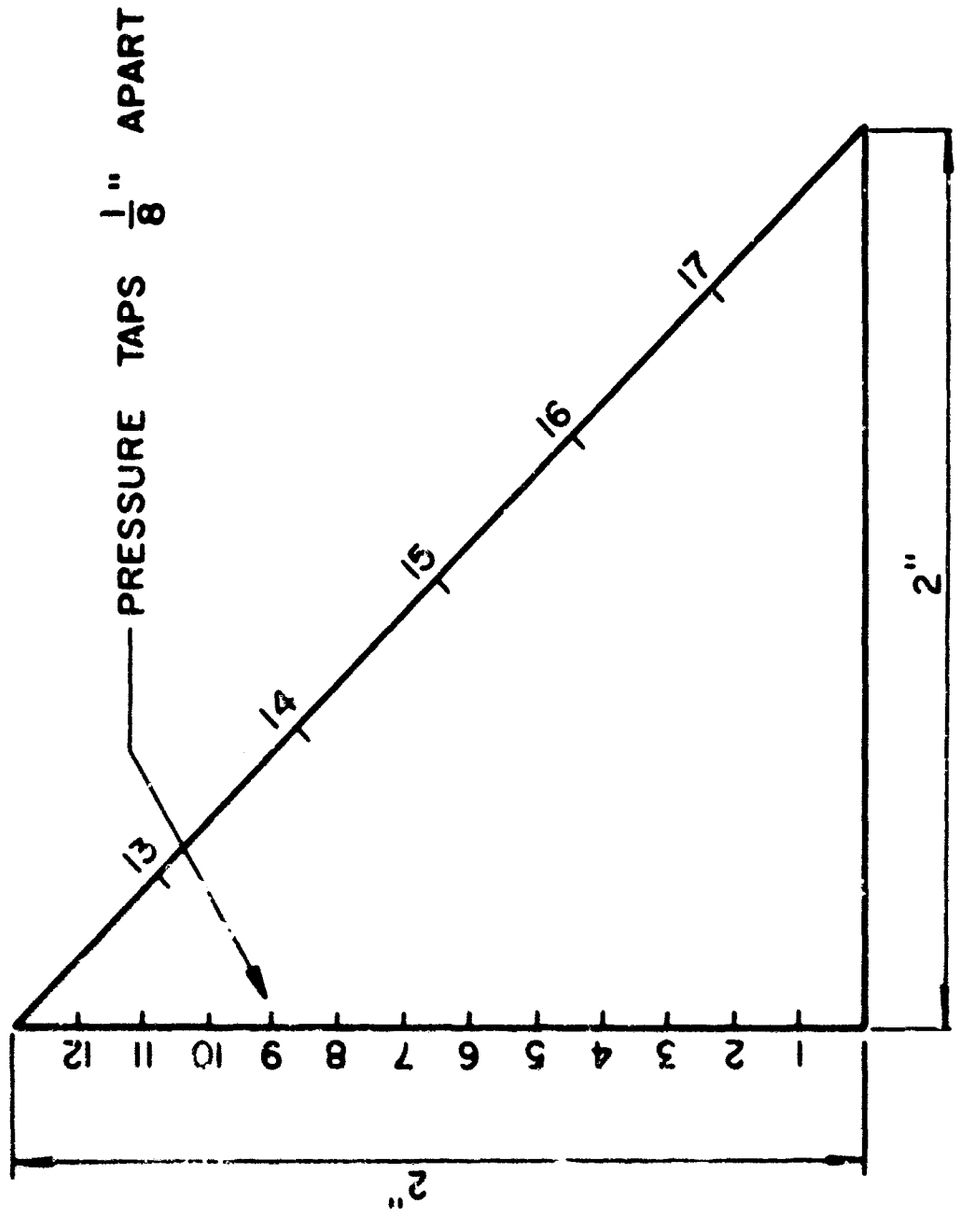

FIG. 4 WEDGE 2" x 2"

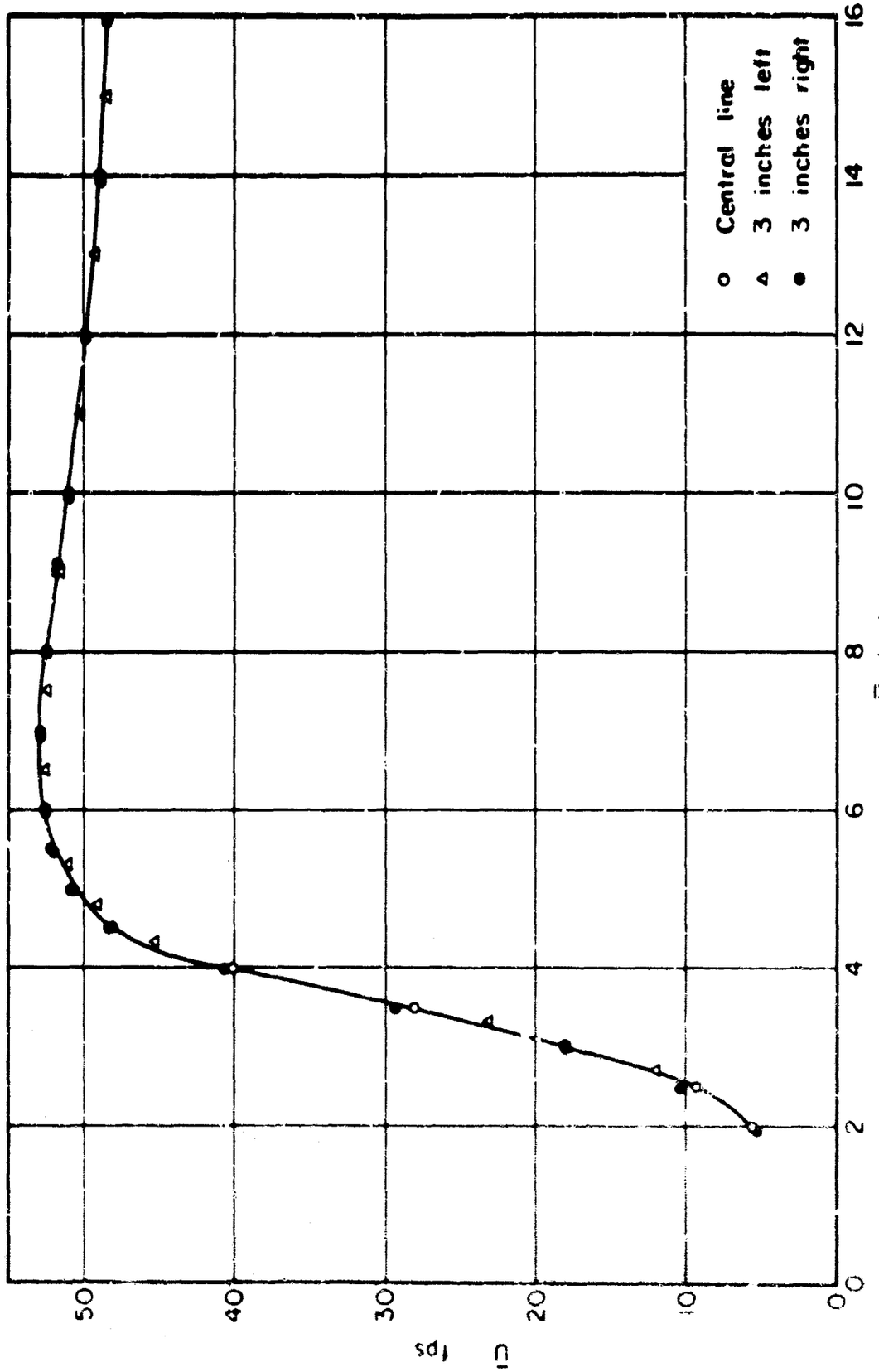

Fig. 5 Velocity profiles at X = 5" behind the wedge hill

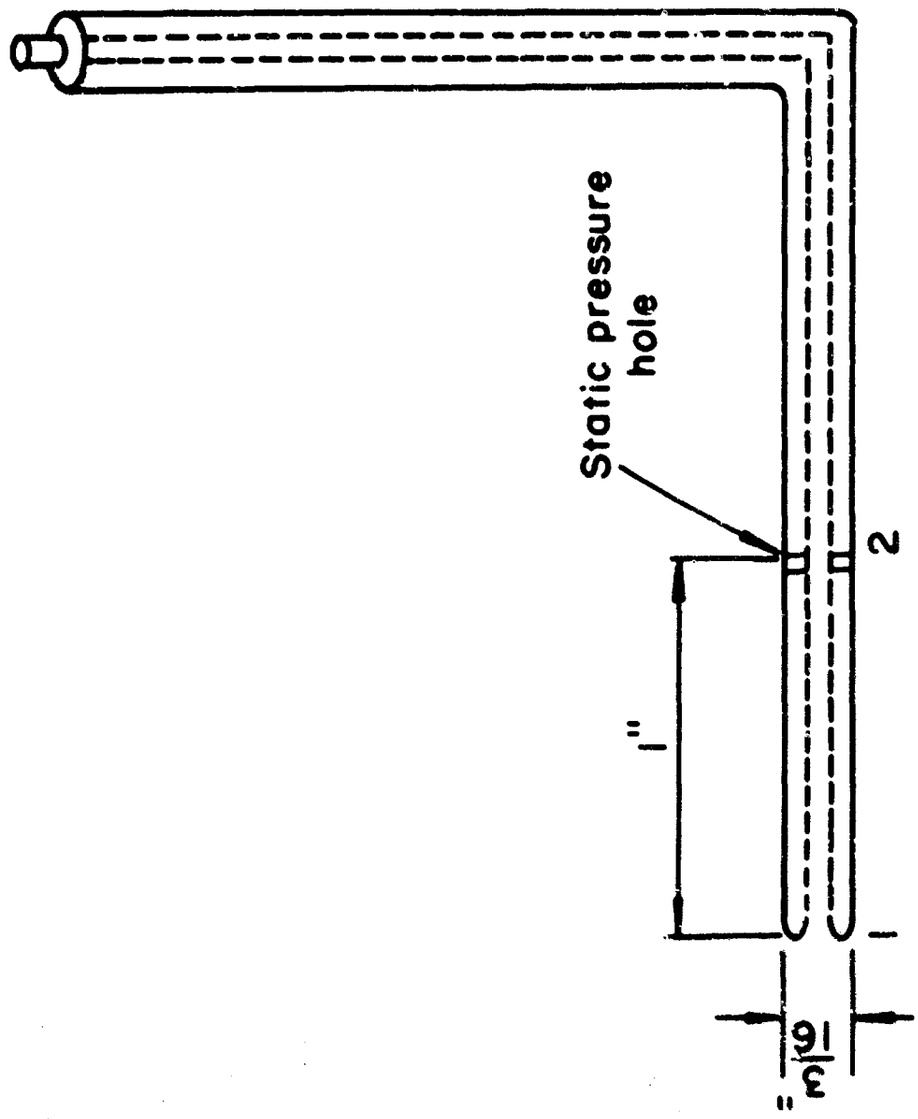

FIG. 6 PITOT TUBE

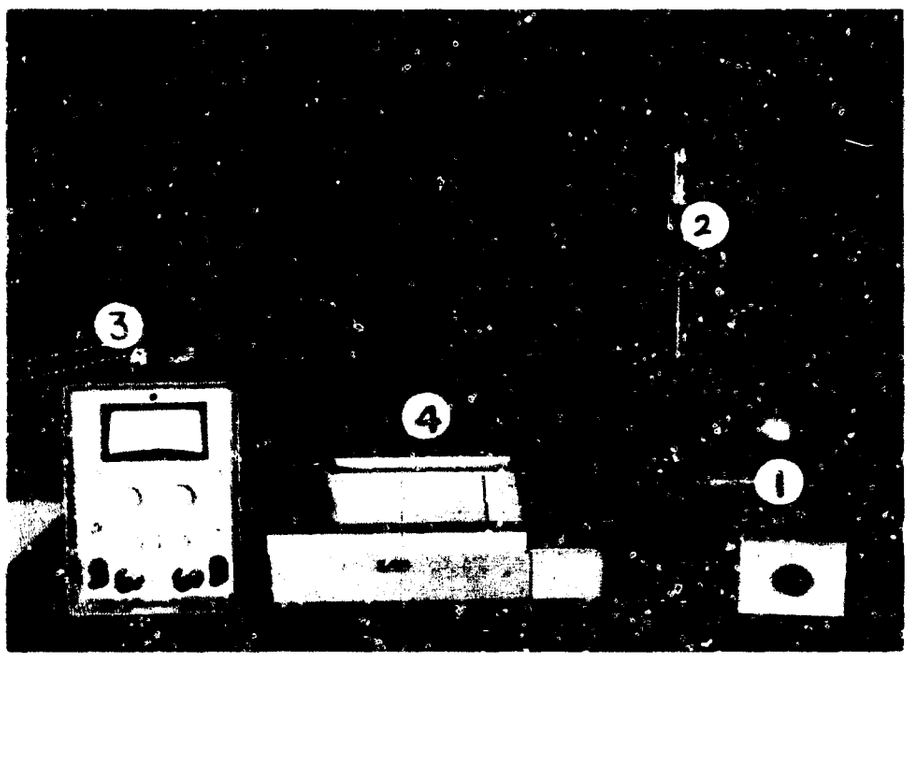

1. Control box
2. Carriage
3. Electronic manometer
4. X-Y plotter

Fig. 7. Pressure measuring equipment

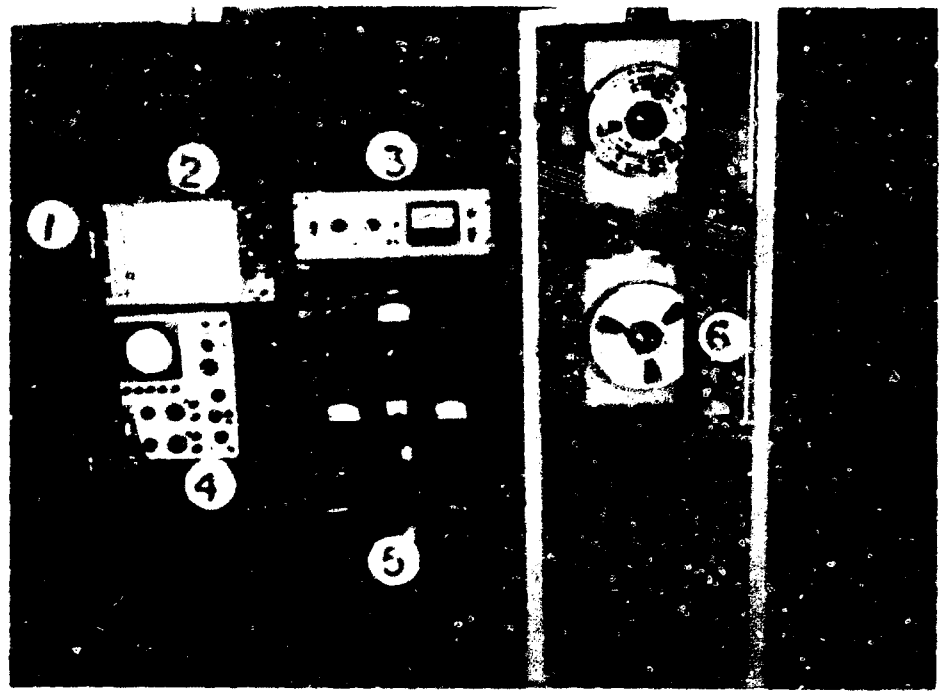

1. Carriage
2. X-Y plotter
3. True rms-meter
4. Electronic manometer
5. Hubbard hot-wire anemometer amplifier
6. Magnetic tape recorder

Fig. 8. Turbulence measuring equipment

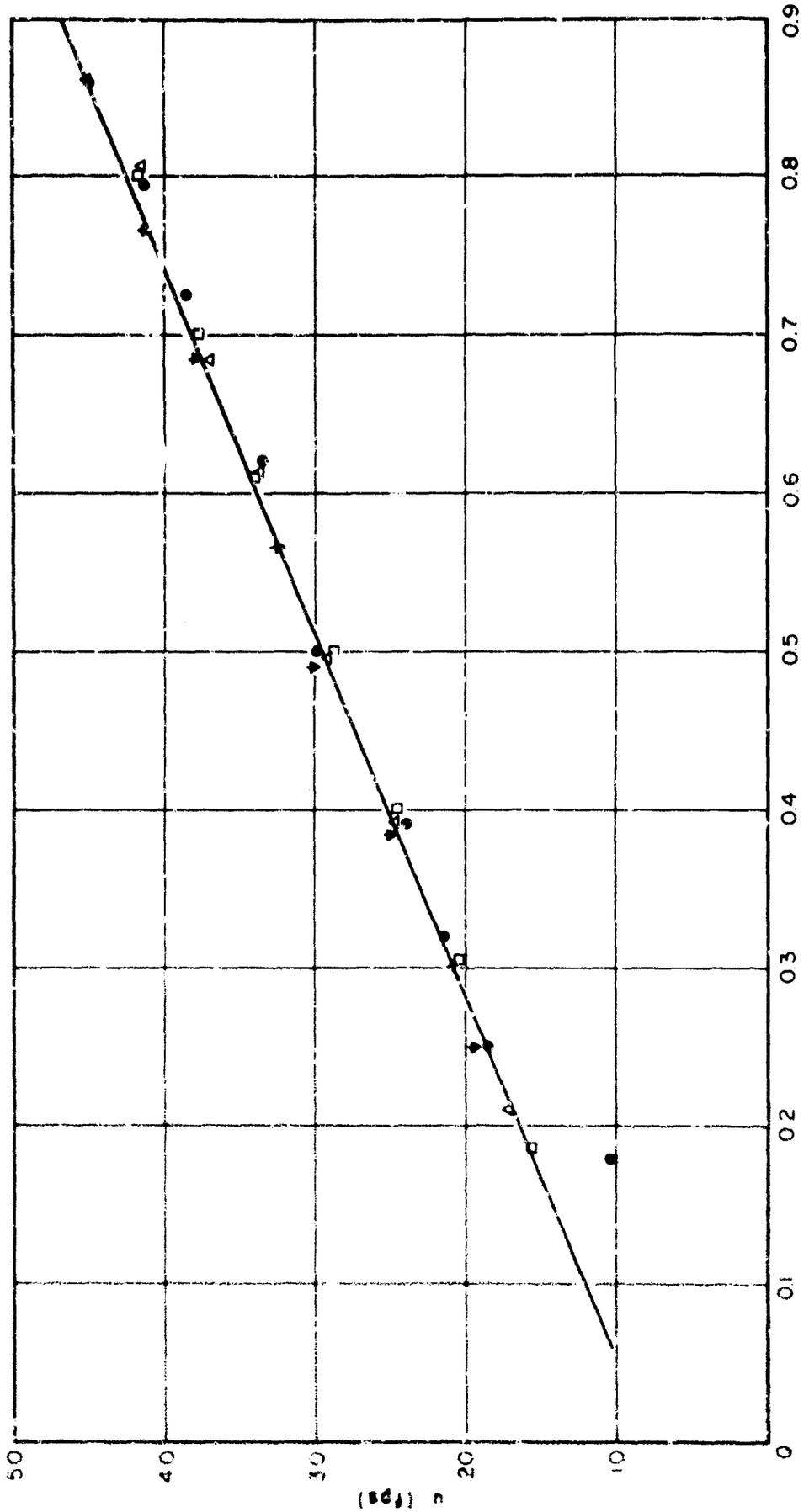

FIG. 9 CALIBRATION CURVE OF HOT WIRE

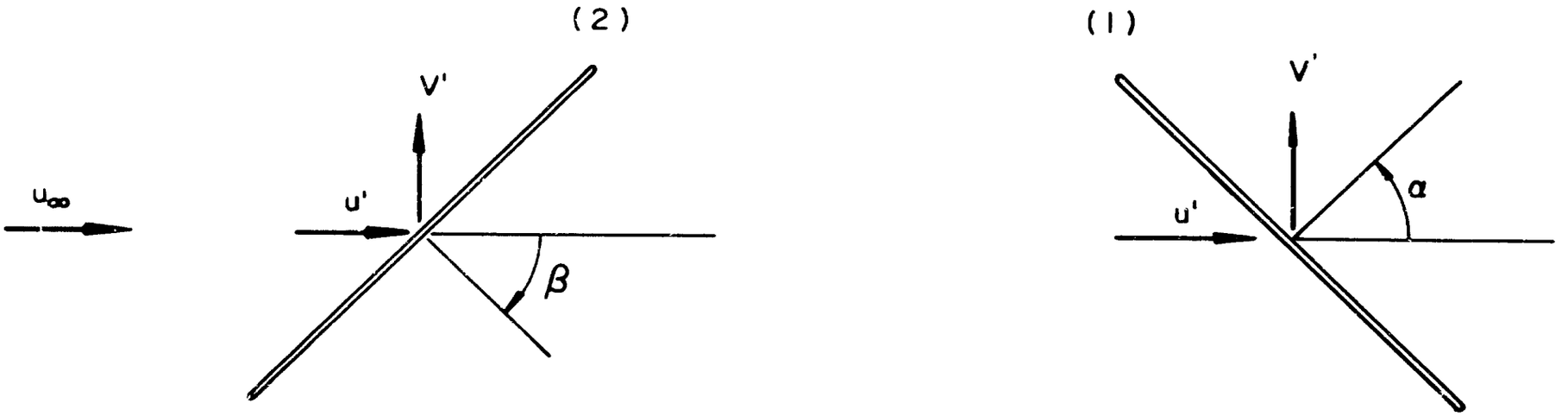

FIG. 10 CROSS WIRE WITH INCLINED ANGLE α AND β

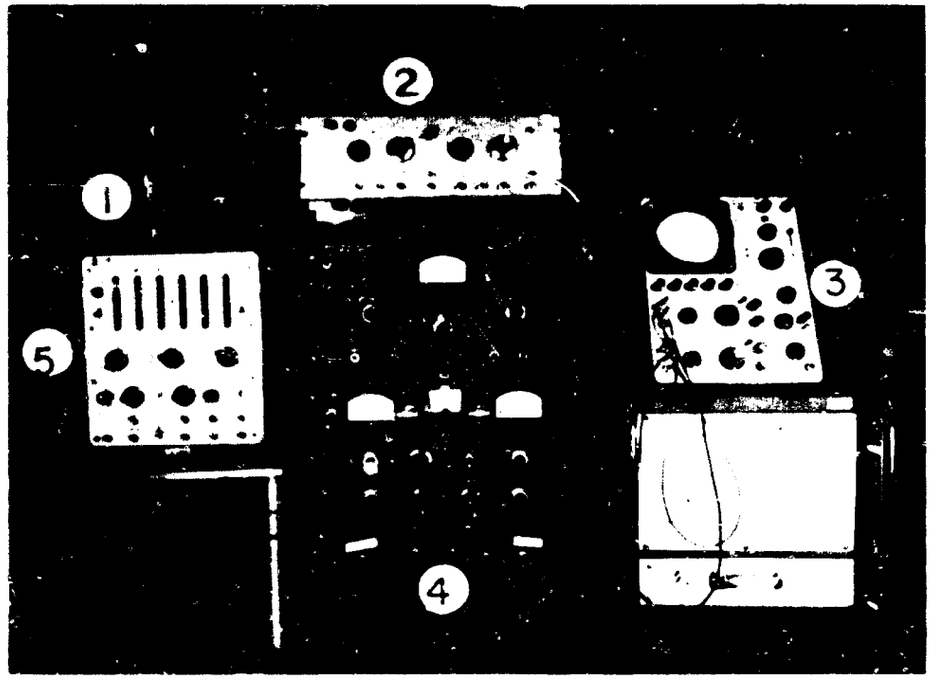

1. Dual wire probe
2. Discriminator circuit
3. Electronic manometer
4. Hubbard hot-wire anemometer amplifier
5. Frequency counter

Fig. 11. Equipment used in measuring reattachment point

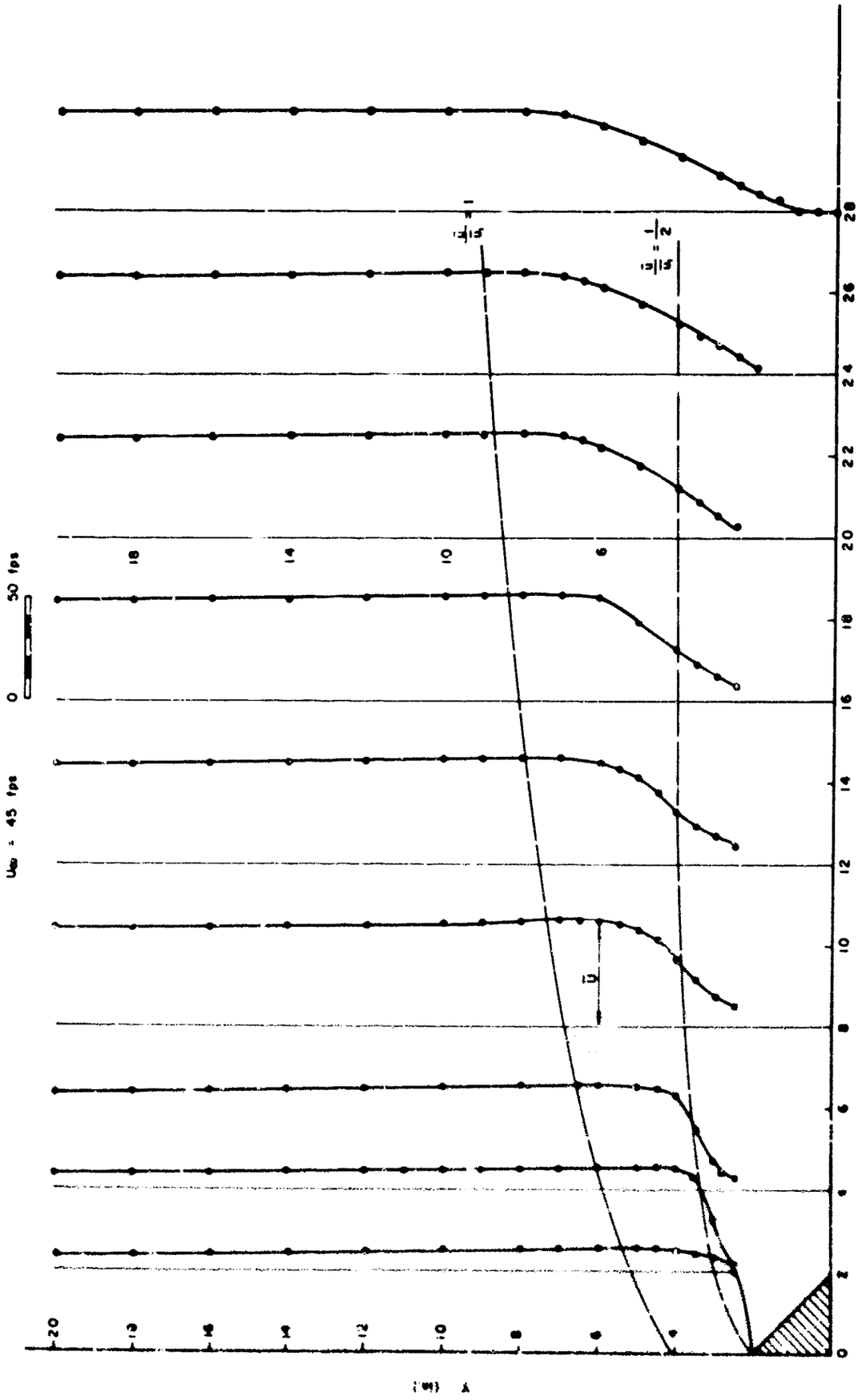

FIG 12 MEAN VELOCITY DISTRIBUTION BEHIND THE 2" x 2" WEDGE HILL

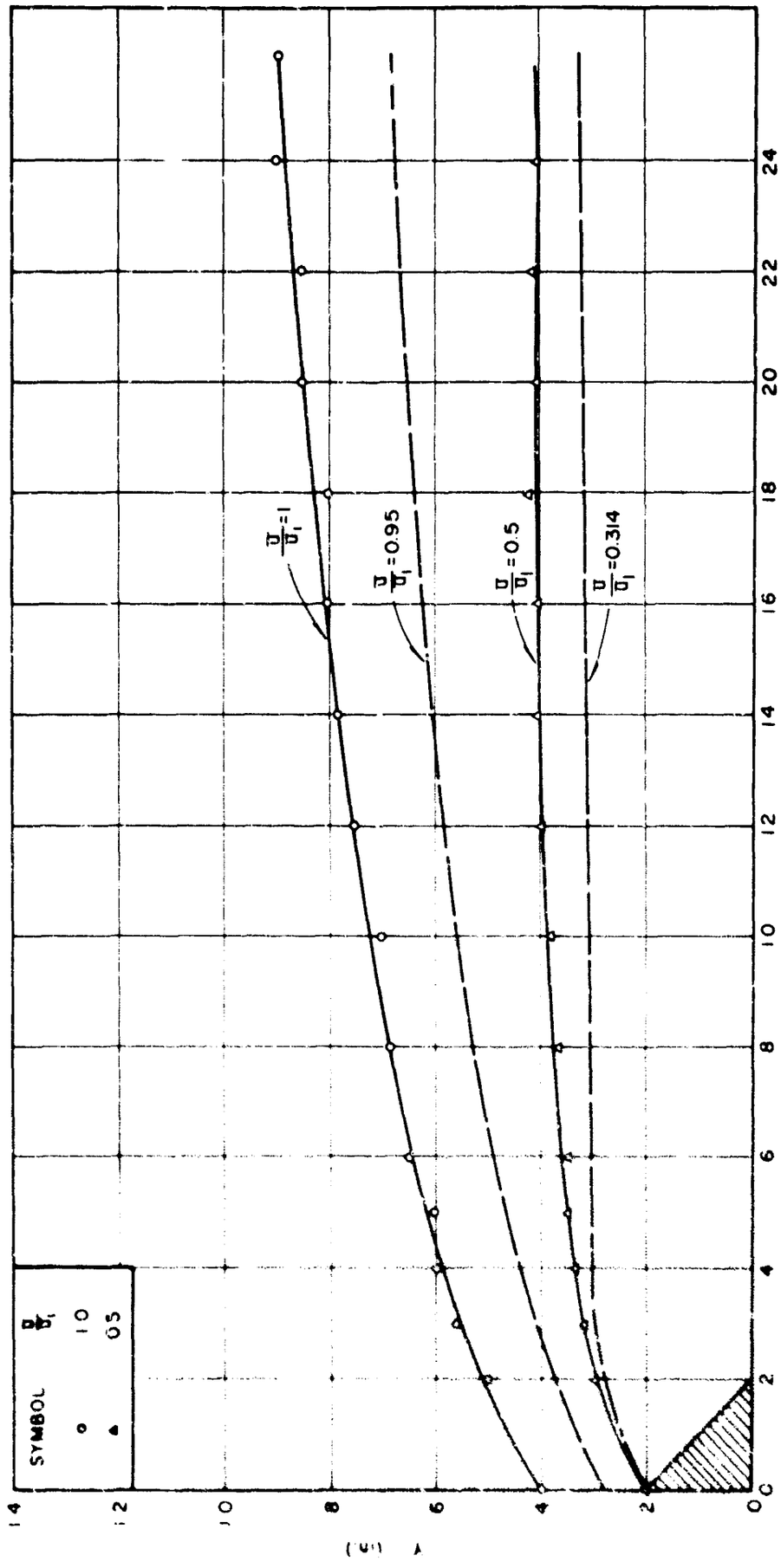

FIG. 13 UPPER JET BOUNDARY AND JET-AXIS WITH U_∞ = 45 fps

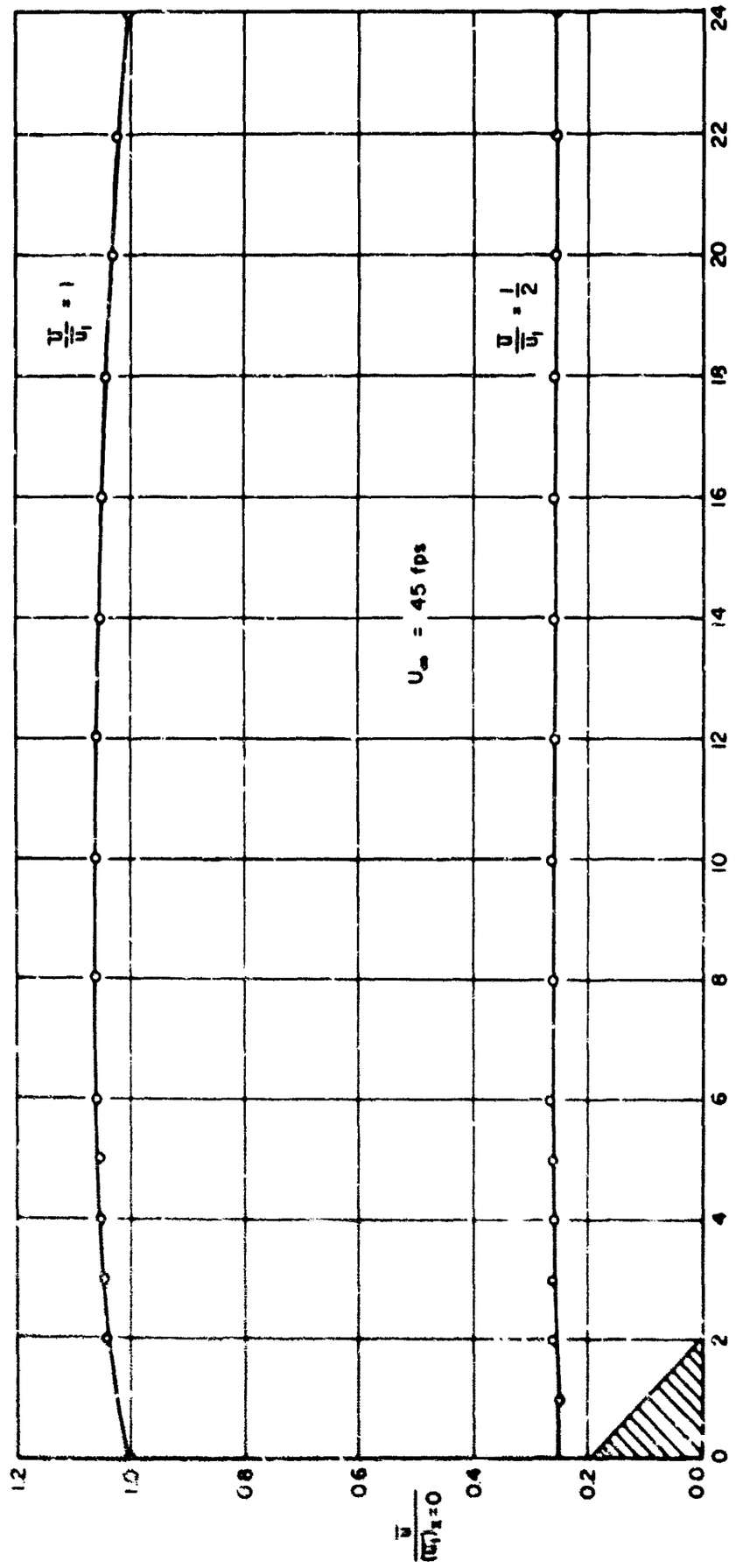

FIG. 14 VARIATION OF VELOCITY ALONG JET BOUNDARY AND JET AXIS.

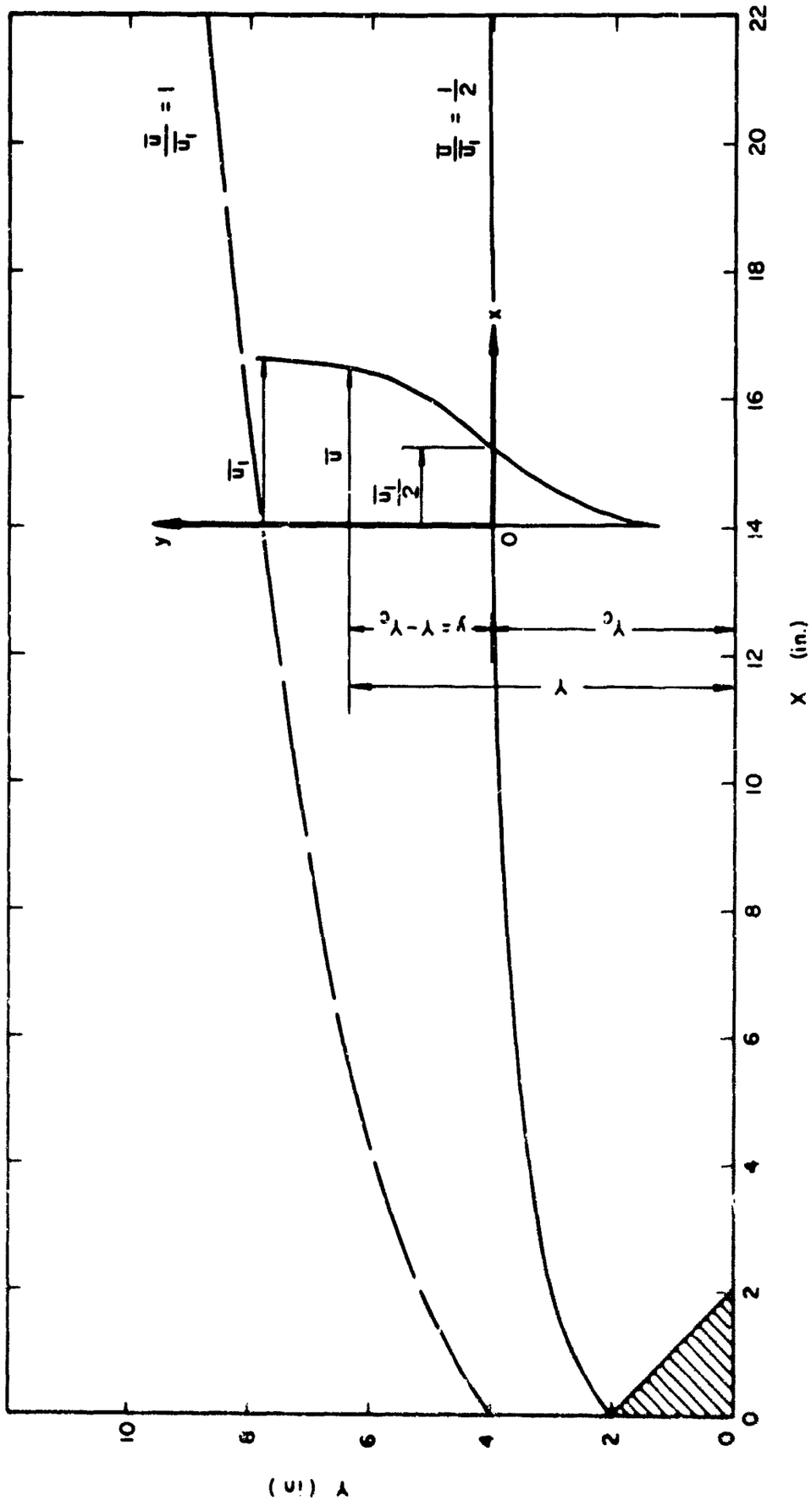

FIG 15 INTRINSIC COORDINATES AND REFERENCE COORDINATES.

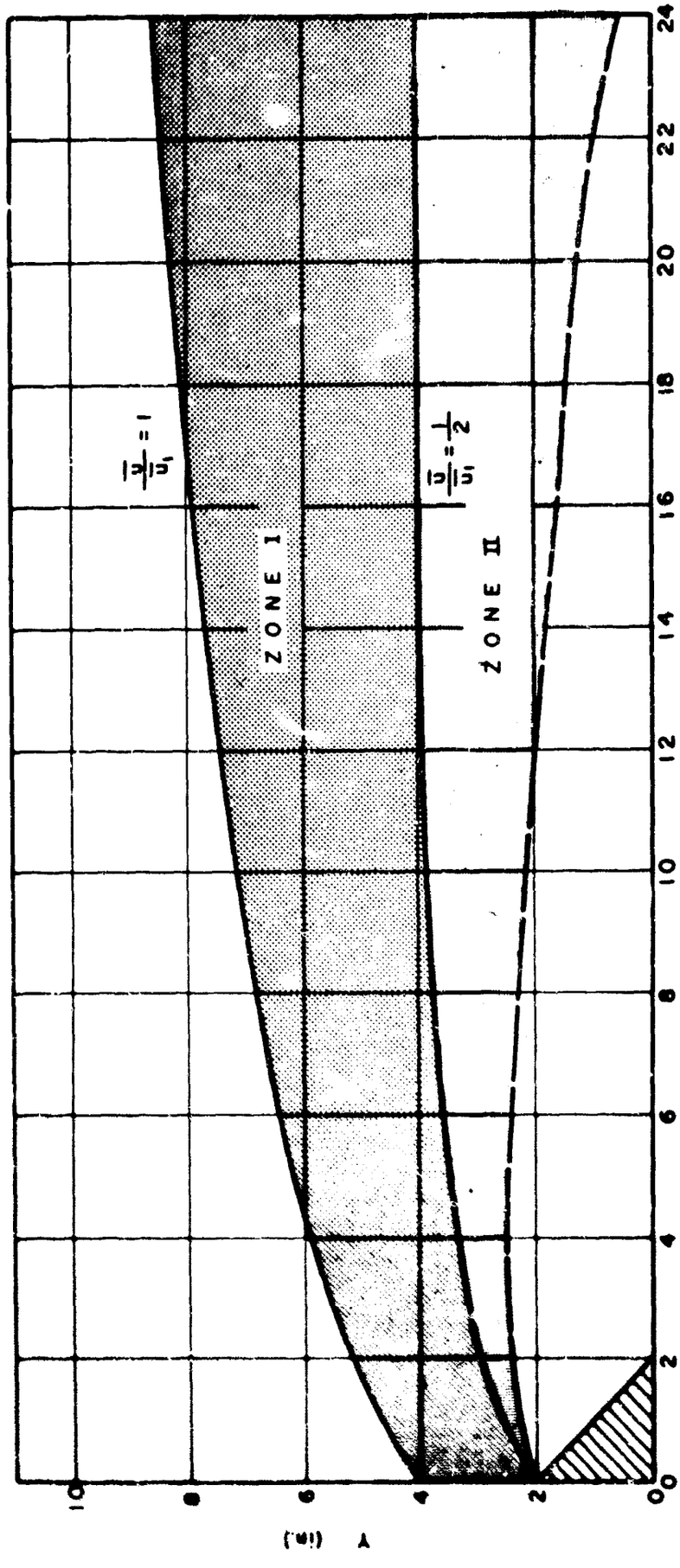

FIG. 16 ZONE I AND ZONE II

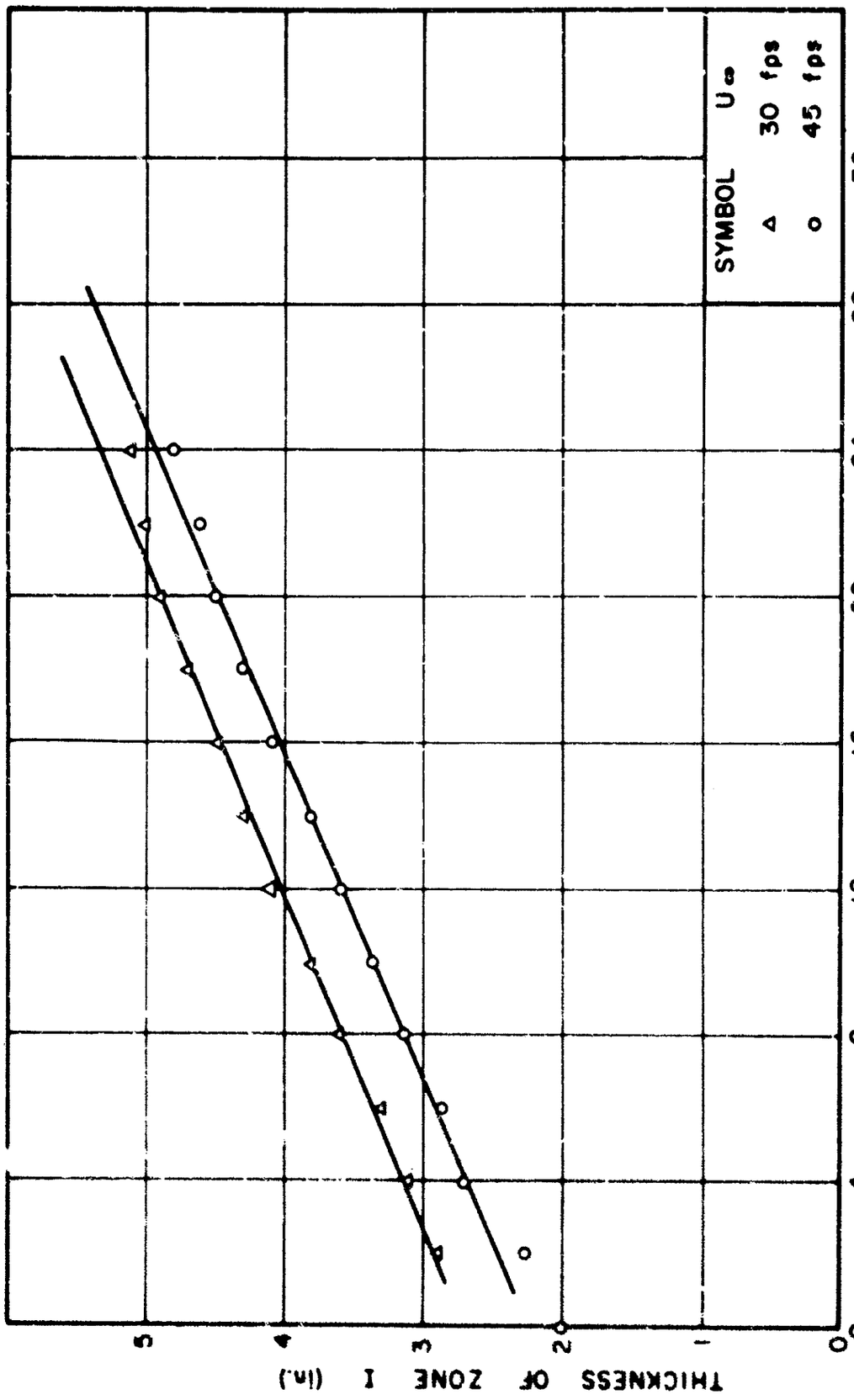

FIG. 17 SPREAD OF THICKNESS OF ZONE I

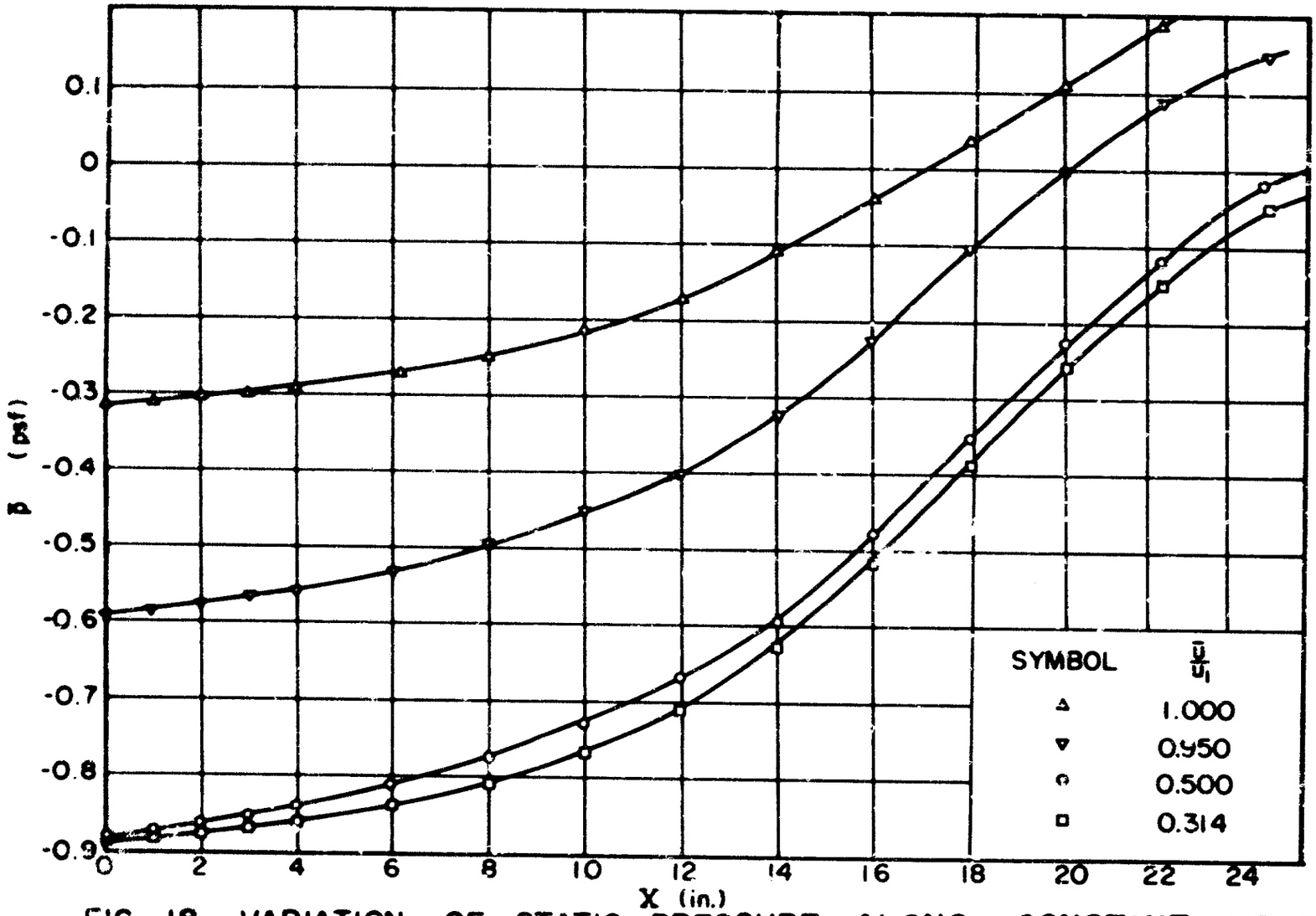

FIG. 18 VARIATION OF STATIC PRESSURE ALONG CONSTANT VELOCITY RATIO LINE FOR U_∞ = 45 fps

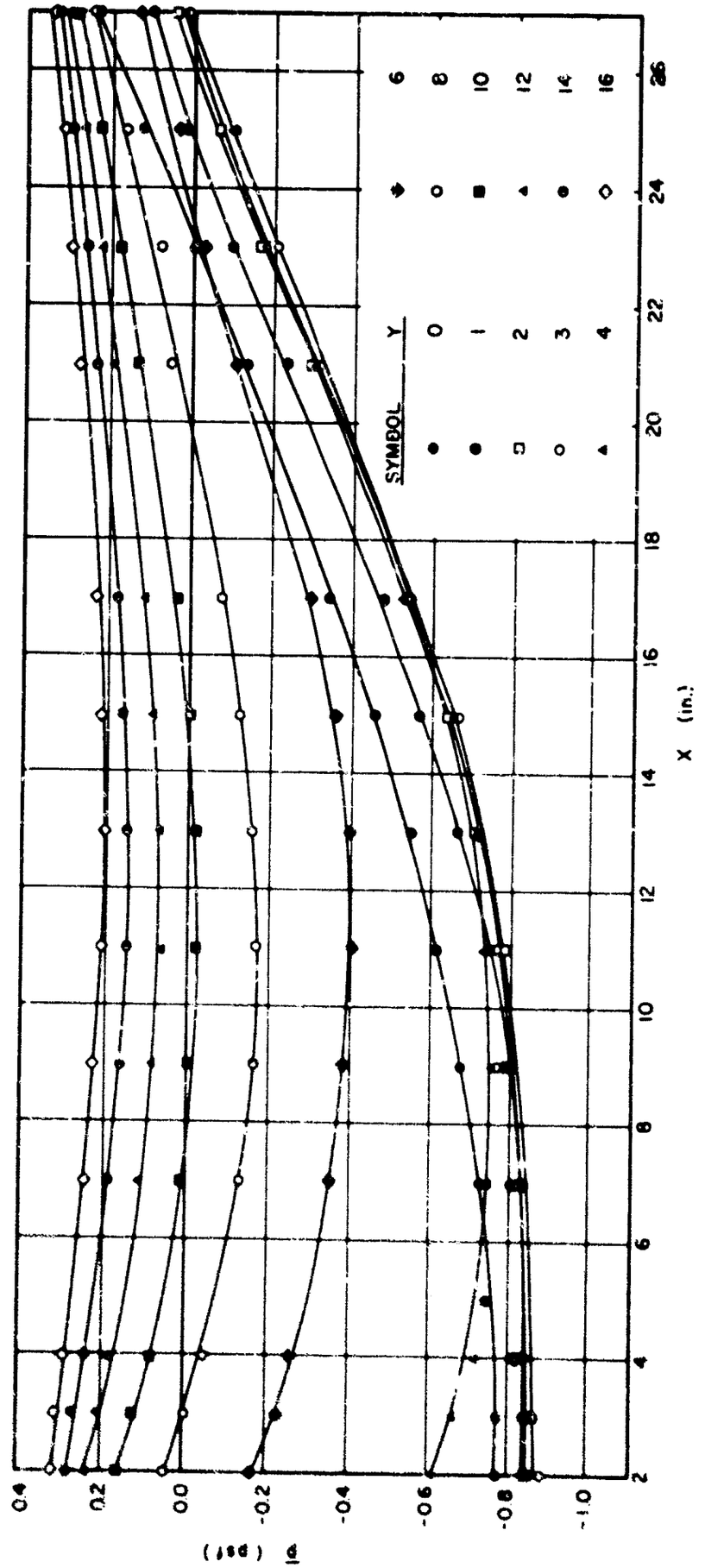

FIG. 19 VARIATION OF STATIC PRESSURE AT CONSTANT HEIGHTS ABOVE THE FLOOR WITH U_∞ = 45 fps

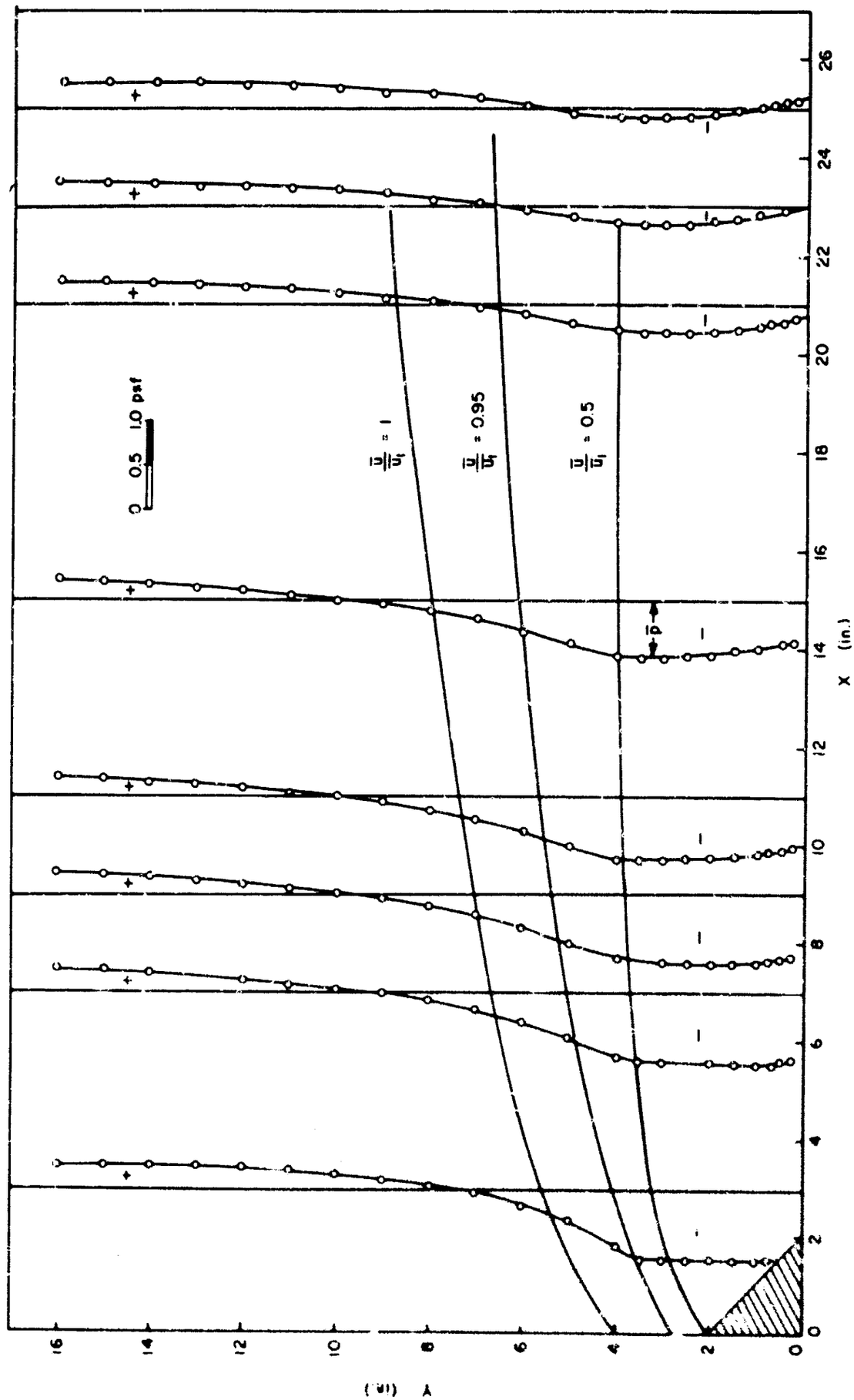

FIG. 20 DEVELOPMENT OF STATIC PRESSURE BEHIND THE HILL WITH U_∞ = 45 fps.

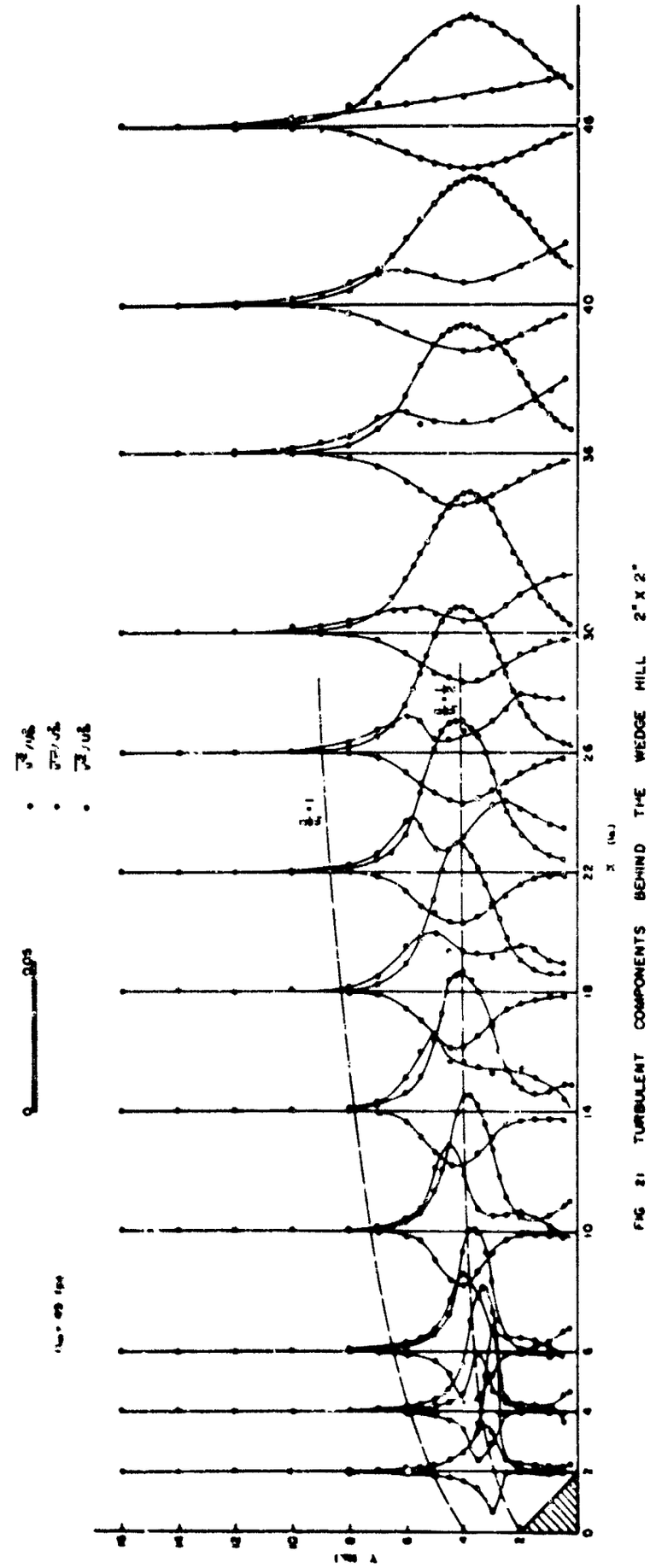

FIG 21 TURBULENT COMPONENTS BEHIND THE WEDGE HILL 2" X 2"

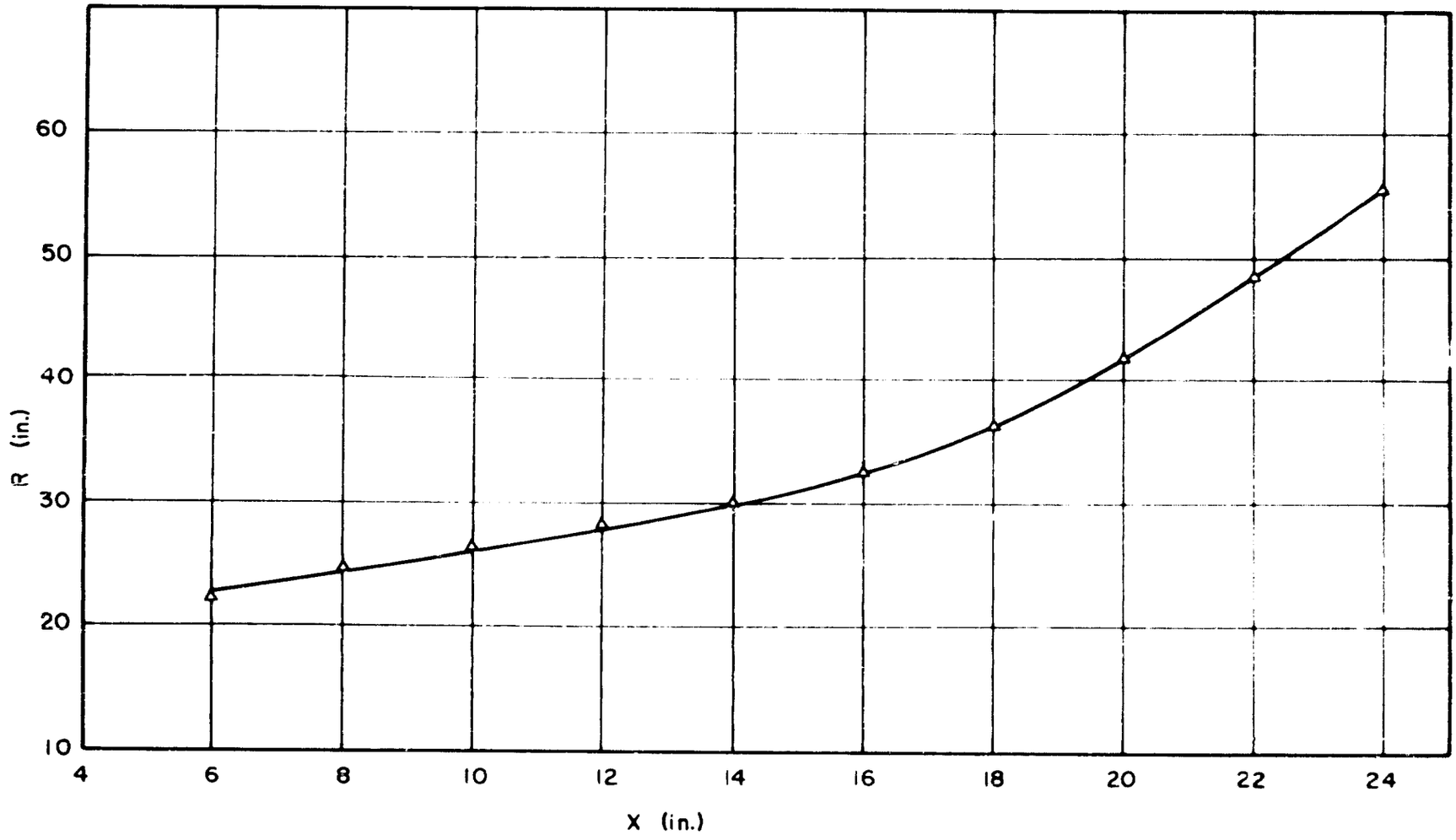

FIG. 22 VARIATION OF RADIUS OF CURVATURE R WITH X U_∞ = 45 fps

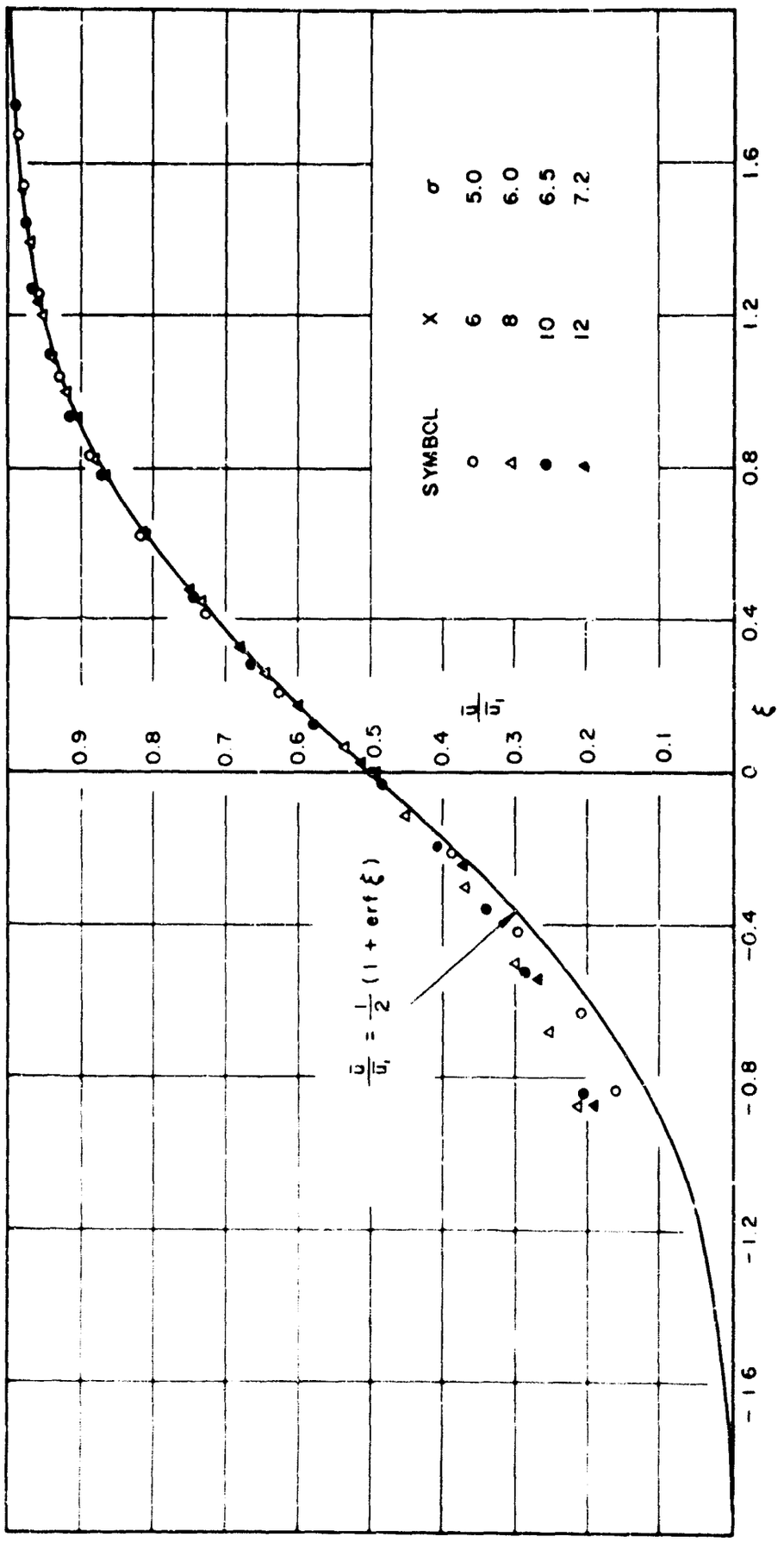

FIG 23-1 COMPARISON OF THEORY AND VELOCITY MEASUREMENTS FOR U_∞ = 45 fps

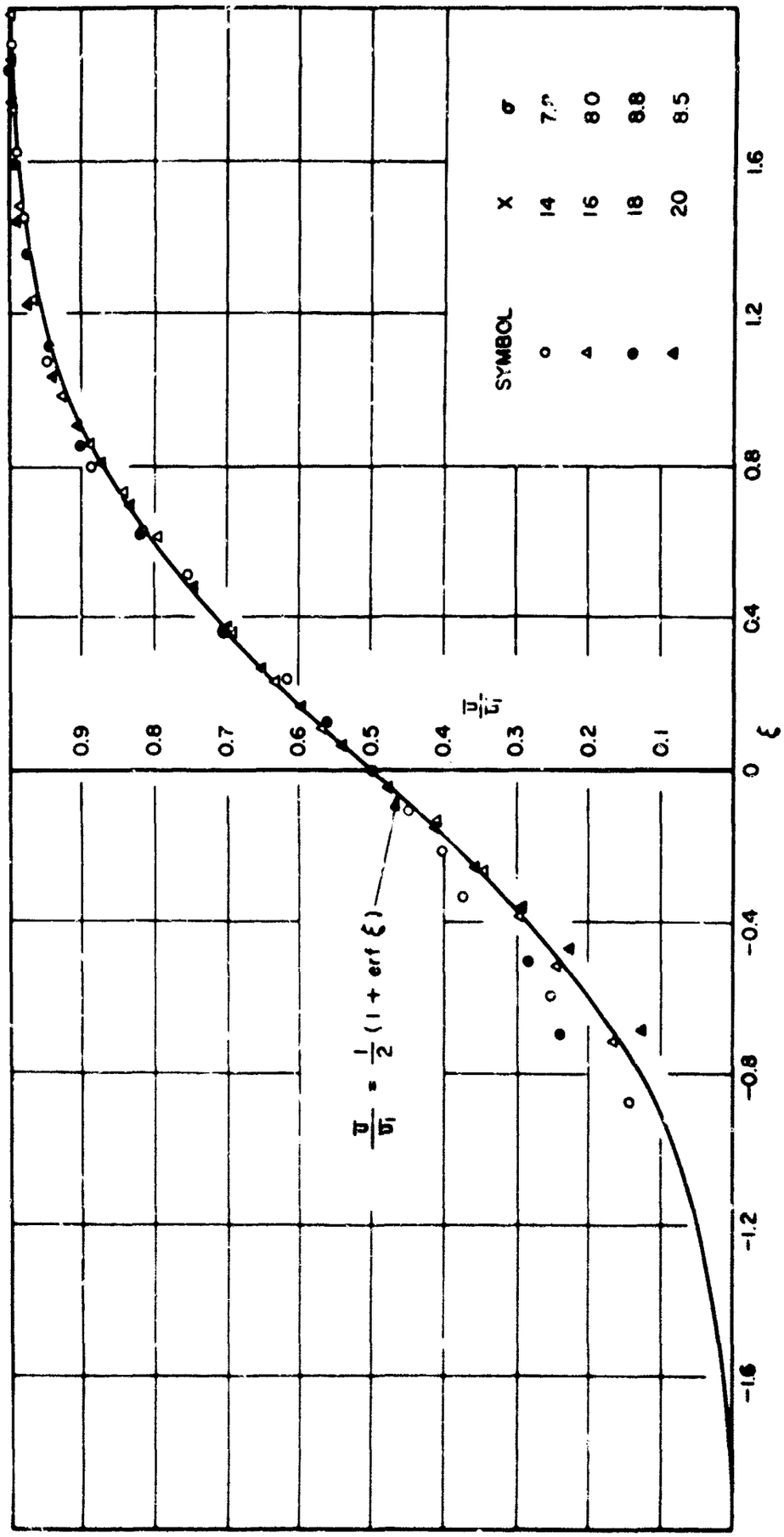

FIG. 23-2 COMPARISON OF THEORY AND VELOCITY MEASUREMENTS FOR U_∞ = 45 fps.

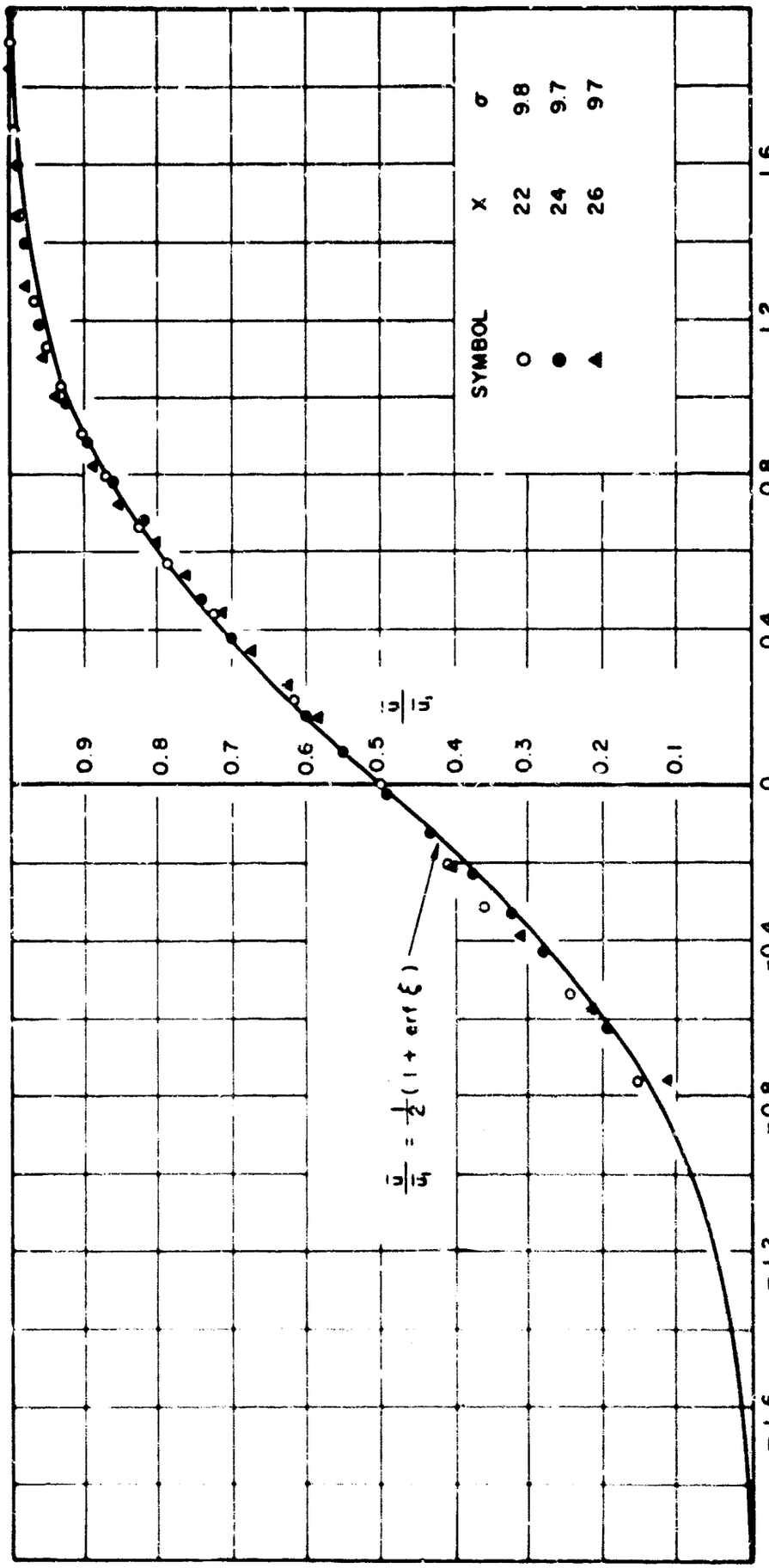

FIG 23-3 COMPARISON OF THEORY AND VELOCITY MEASUREMENTS FOR U_∞ = 45 fps

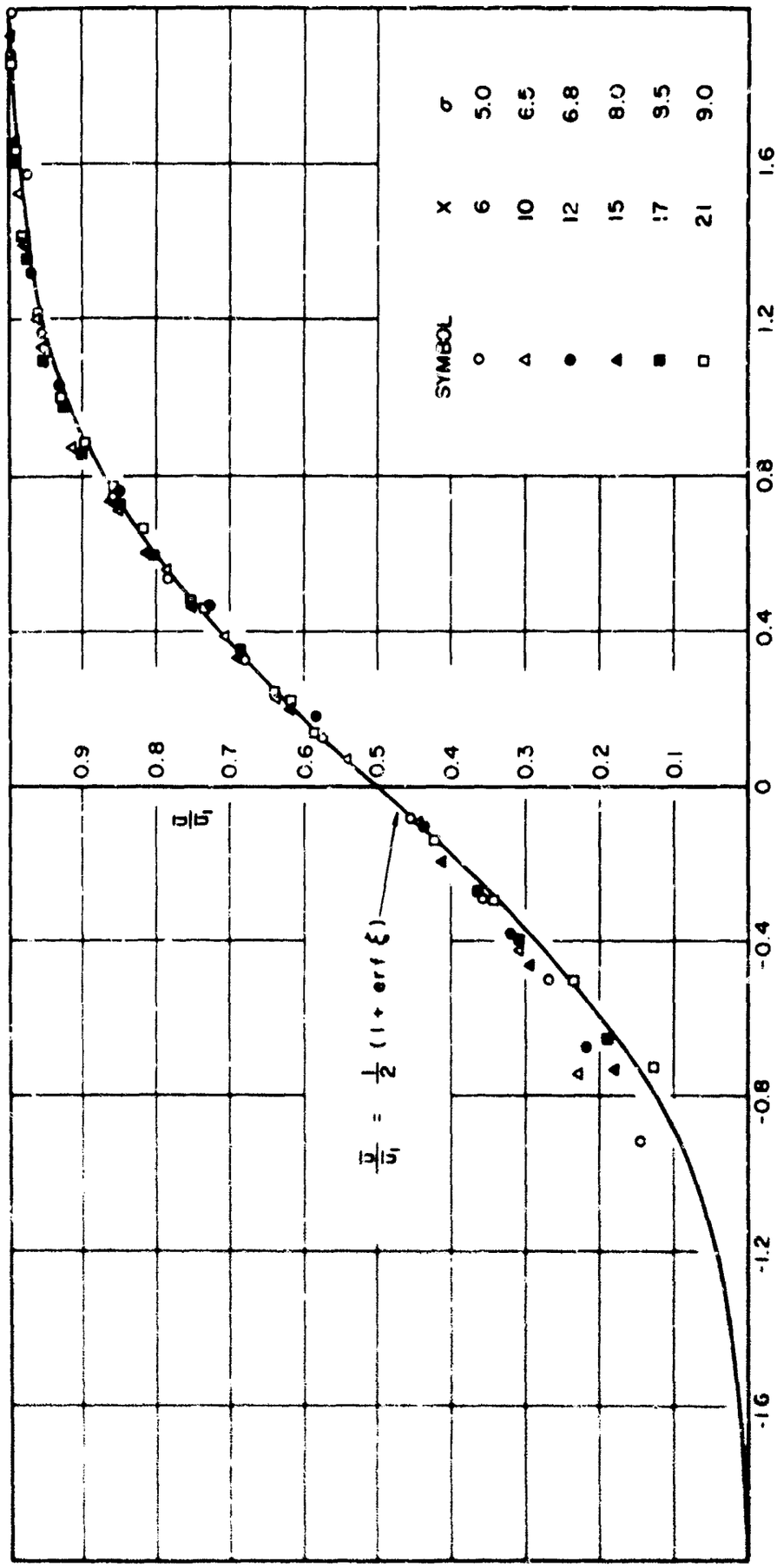

FIG. 23-4 COMPARISON OF THEORY AND VELOCITY MEASUREMENT FOR U_∞ = 30 fps

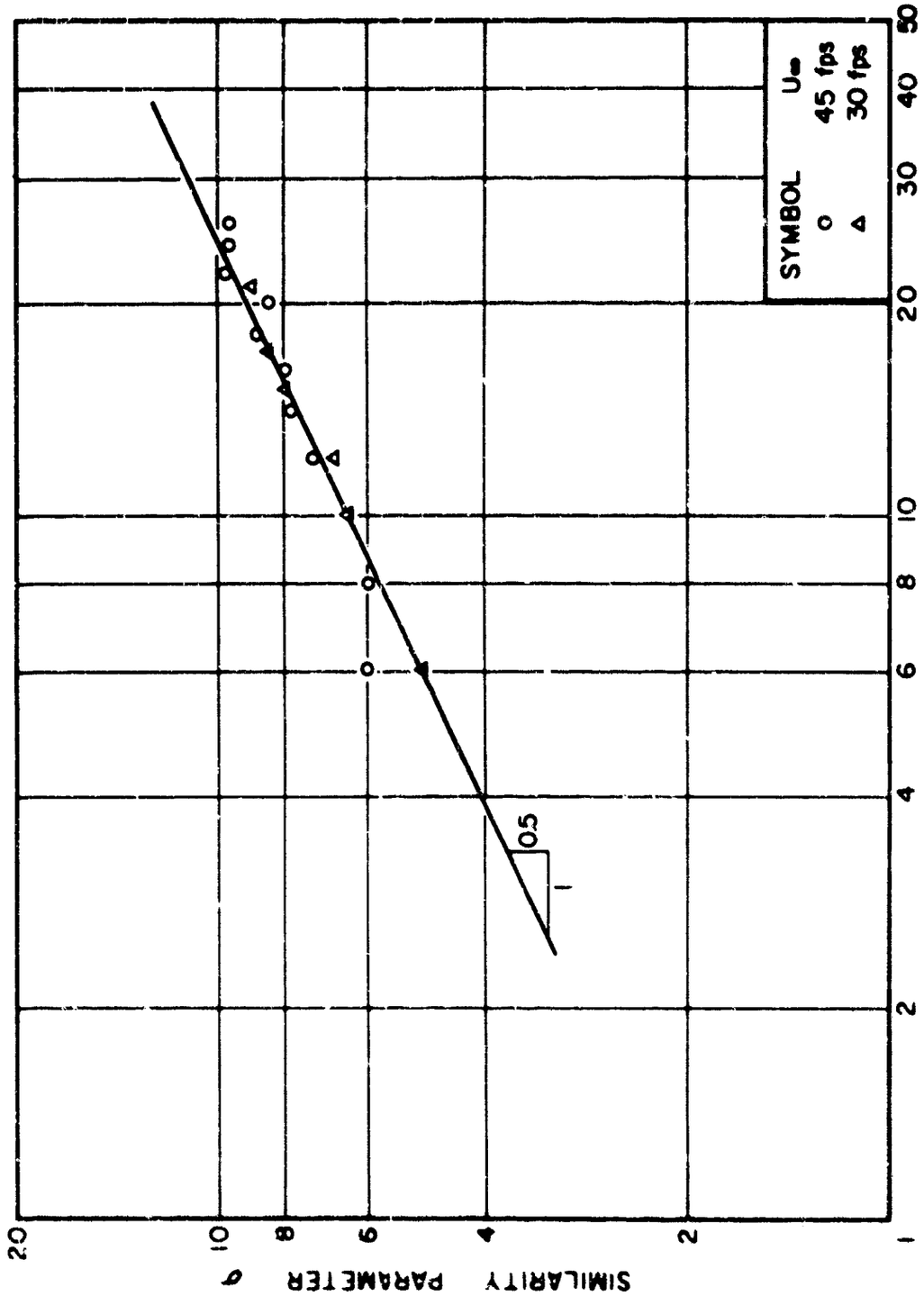

FIG. 24 VARIATION OF SIMILARITY PARAMETER σ WITH DISTANCE X

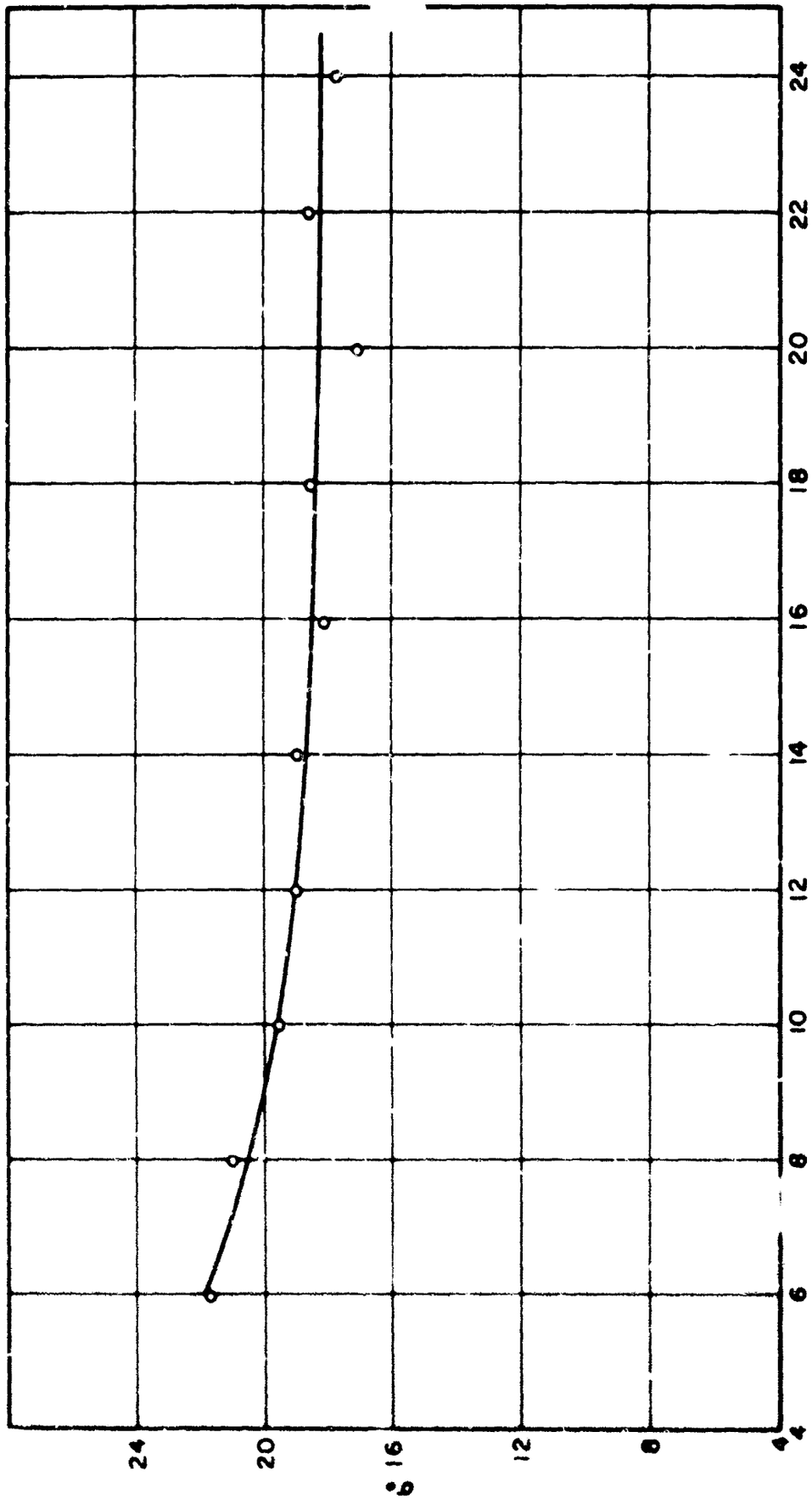

FIG. 25 VARIATION OF δ^* WITH X FOR U_∞ = 45 fps

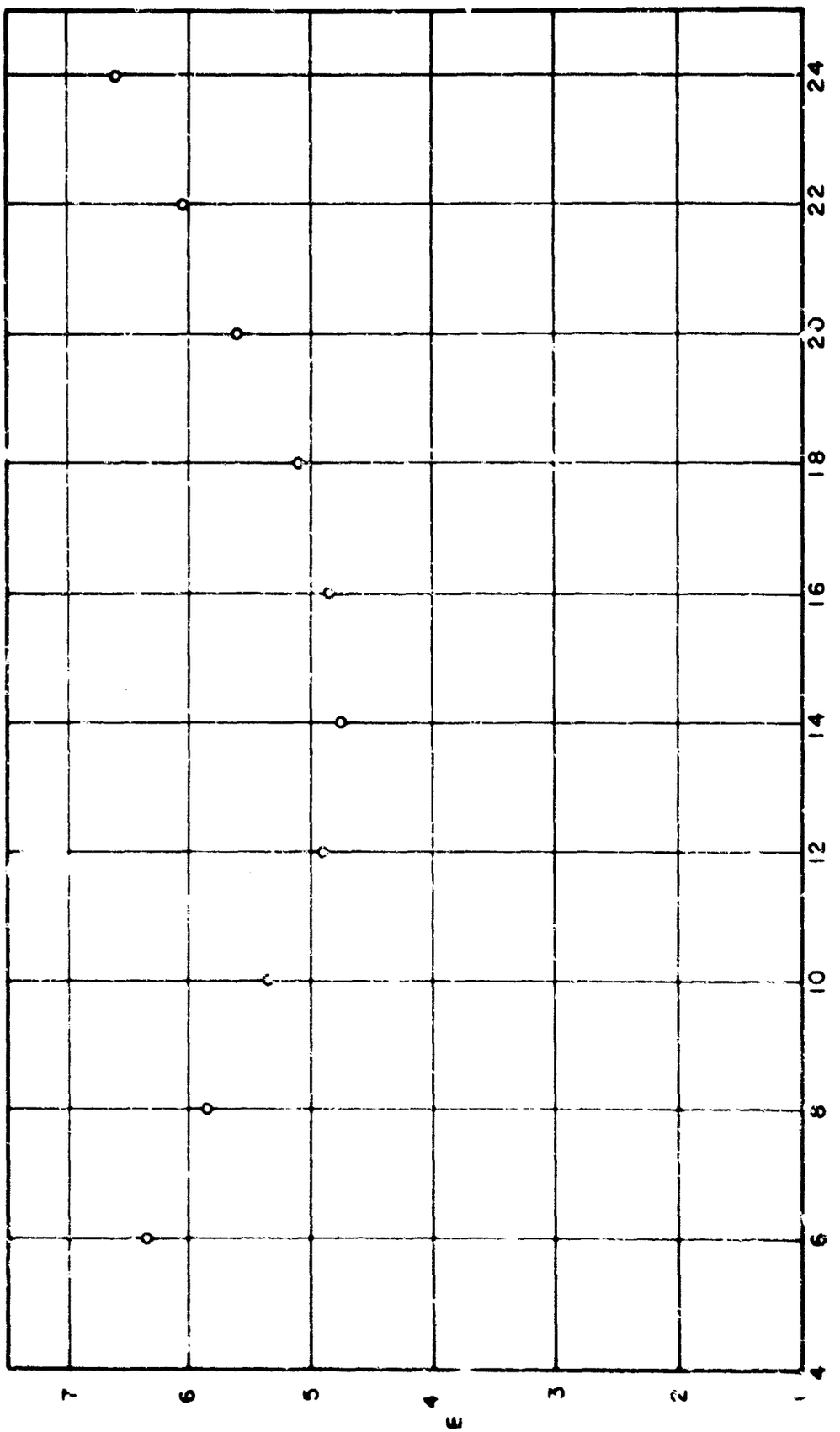

FIG. 26 VARIATION OF m WITH X